Amanzi Theory Guide,
Mathematical Modeling Requirements

October 8, 2024

AMANZI-SRD, Revision 1.0

United States Department of Energy

V. Gyrya, LANL K. Lipnikov, LANL D. Moulton, LANL S. Molins, LBNL
C. Steefel, LBNL

LA-UR-20-22486

This version of the Software Requirements Document (SRD) is based on the *"Mathematical Formulation Requirements and Specification for the Process Models"*, version ASCEM-HPC-2011-01-0c, which was developed for the by ASCEM project by:

C. Steefel, LBNL	P. Lichtner, LANL	J. Bell, LBNL	G. Zyvoloski, LANL
D. Moulton, LANL	T. Woley, LLNL	G. Moridis, LBNL	B. Andre, LBNL
G. Pau, LBNL	D. Bacon, PNNL	S. Yabusaki	L. Zheng, LBNL
K. Lipnikov, LANL	N. Spycher, LBNL	E. Sonnenthal, LBNL	J. Davis, LBNL
J. Meza, LBNL			

DISCLAIMER

Table of Contents

List of Tables

List of Figures

1 Introduction to Process Models Requirements

1.1 Overview

NEEDS TO BE WRITTEN

1.2 Purpose and Scope of this Document

At the highest level of the HPC Simulator design is a set of process models that mathematically represent the physical, chemical, and biological phenomena controlling contaminant release into, and transport in, the subsurface. The objective of this requirements document is to provide a catalogue of process models, along with their detailed mathematical formulation, for potential implementation in the HPC Simulator. This concise mathematical description and accompanying analysis, provides critical information for requirements and design of both the HPC Core Framework (Task 1.1.2.2) and the HPC Toolsets (Task 1.1.2.3).

It is important to note that with its focus on mathematical descriptions for a catalogue of process models, this requirements document is significantly different from a traditional Software Requirements Specification (SRS) document. Hence, this document does not follow the IEEE Std 830-1998 template, and instead uses a process category based layout that is summarized in Section 1.3. Moreover, this mathematical focus serves multiple audiences:

1. This document provides guidance to the developers engaged in designing and implementing the HPC Core Framework and HPC Toolsets. To meet their needs, sufficient detail for each process model is provided in the form of a background discussion, supporting equations, and references to relevant literature.

2. The document is also intended for "domain scientists" whose primary interest is in the processes themselves. The presentation is intended to justify the choice of process models and their mathematical detail.

3. Finally, the document is also intended for end users engaged in individual site applications.

Over time this document will evolve into a comprehensive graded presentation of models, from complex to simple, under a general mathematical framework for each process category. Evolution of the list of processes is inevitable, and the modular design of the HPC Simulator will easily accommodate the addition of new process implementations.

1.3 Organization and Layout of this Document

The remainder of this document is organized based on individual process category. These include presentation of *Isothermal Flow Processes* in Section 2, *Thermal Processes* in Section 3, *Transport Processes* in Section 4, and *Biogeochemical Reaction Processes* in Section 5. Each of these process categories may present multiple process models.

In Section 2, *Isothermal Flow Processes*, we consider models of fluid flow at constant temperature. We limit ourselves to the case of a single fluid phase, i.e. no water-oil flows. Based on the saturation levels we use one of two models: fully saturated and partially saturated flows. Further, use of Richards Equation requires certain assumptions on the gas phase not moving.

In Section 3, *Thermal Processes*, we discuss extension of the models of Section 2 to the case of changing temperature by adding a concervation of energy equation.

In Section 4, *Transport Processes*, we consider models for transport, i.e. evolution of distributions, of solute species. Each of the species can be part of either gas, fluid or solid phase. In the solid phase specied do not move. In the gas phase species can only diffuse (due to the assumptions of Richards equation). In the fluid phase the transport of the species is affected by the fluid flow as well as dispersion and diffusion processes. In this section we also consider a dual porocity models, designed to capture the difference in fluid motion in the cracks and pores.

In Section 5, *Biogeochemical Reaction Processes*, we consider a variety of biochemical reaction processes, which from the point of view of model equations convert one species into others and result in various heat sources.

The notational conventions and variables used throughout the document are summarized in Section 1.4.

1.4 Variables and Notations

In this section we list all the variables used throughout the rest of the document. In particular, for multiple variables we use subscript l, s and g to indicate that the particular quantity is the property of the *liquid*, *solid* or *gas*, respectively. We also use subscripts m and f to indicate quantities that are attributed to the *matrix*/pores and *fracture*, respectively.

Table 1: List of global variables.

Symbol	Meaning	Units
C_i	concentration of ith species	$\mathrm{mol} \cdot \mathrm{m}^{-3}$
e_l	enthalpy of the liquid	m
$\boldsymbol{g}$	gravity vector	$\mathrm{m} \cdot \mathrm{s}^{-2}$
g	gravity magnitude	$\mathrm{m} \cdot \mathrm{s}^{-2}$
h	hydrolic head	m
$\boldsymbol{J}$	generic flux	$\mathrm{mol} \cdot \mathrm{m}^{-2} \cdot \mathrm{s}^{-1}$
$\mathbb{K}$	absolute permeability tensor	m^2
k_{rl}	relative permeability	$-$
p_l	liquid pressure	Pa
$\boldsymbol{q}$	Darcy velocity	$\mathrm{m} \cdot \mathrm{s}^{-1}$
S_s	specific storage	m^{-1}
S_y	specific yield	$-$
s_l	liquid saturation	$-$

Continued on next page

Table 1 – Continued

Symbol	Meaning	Units
u_l	internal energy of the liquid	$\mathrm{kg} \cdot \mathrm{m}^2 \cdot \mathrm{s}^{-2}$
u_r	internal energy of the rock	$\mathrm{kg} \cdot \mathrm{m}^2 \cdot \mathrm{s}^{-2}$
μ_l	liquid viscosity	$\mathrm{Pa} \cdot \mathrm{s}$
ρ_l	liquid density	$\mathrm{kg} \cdot \mathrm{m}^{-3}$
ϕ	porosity	$-$
ϕ_f	porosity of fracture	$-$
ϕ_m	porosity of matrix	$-$
η_l	molar liquid density	$\mathrm{mol} \cdot \mathrm{m}^{-3}$
θ	volumetric water content	$\mathrm{mol} \cdot \mathrm{m}^{-3}$
θ_f	volumetric water content of fracture	$\mathrm{mol} \cdot \mathrm{m}^{-3}$
θ_m	volumetric water content of matrix	$\mathrm{mol} \cdot \mathrm{m}^{-3}$

2 Isothermal Flow Processes

2.1 Overview

Subsurface flow simulations typically assume that Darcy's law is valid. As this law gives a relationship between velocity and pressure, it essentially replaces the momentum equation. There has been much research to support the validity of Darcy's Law (Bear, 1972). Most references give the applicability of Darcy's Law to be for laminar flows with Reynolds numbers less that 10 using the pore throat diameter for a soil. There has been some effort to include inertial as well as turbulence effects that can occur near the wells.

It is also assumed that thermodynamic equilibrium (mechanical and thermal) exists for each grid block. Sub-grid scale features often play a prominent role in multi-fluid simulations. Faults and fractures will likely be fast paths for contaminant transport and can effectively be treated with multiple porosity models. Similarly, rate-limited diffusion from clay inclusions can also be modeled with a multiple porosity material.

2.2 Fully Saturated Flow

The most basic flow model is a single-phase fully saturated flow in a porous medium. Notwithstanding its simplicity, it has a wide application to describing subsurface processes.

2.2.1 Assumptions and Applicability

There are many assumptions required for the strict validity of Darcy's Law, including

- incompressibility and
- laminararity of the flow.

We also assume that

- solid/rock is incompressible,
- fluid viscosity is constant,
- there are no fractures, only pores.

2.2.2 Process Model Equations

Under the above assumptions fully saturated flow is governed by

$$\left(\frac{S_s}{g} + \frac{S_y}{L\,g}\right)\frac{\partial p_l}{\partial t} = -\boldsymbol{\nabla}\cdot(\rho_l \boldsymbol{q}_l) + Q, \tag{2.1a}$$

$$\boldsymbol{q}_l = -\frac{\mathbb{K}}{\mu_l}(\boldsymbol{\nabla} p_l - \rho_l \boldsymbol{g}), \tag{2.1b}$$

where the primary variable is the fluid presure p_l [Pa]. The fluid velocity $\boldsymbol{q}_l$ $[\mathrm{m}\cdot\mathrm{s}^{-1}]$ is the dependent variable. All the other variables can be treated as material parameters that sometimes may depend on pressure. These include: S_s $[\mathrm{m}^{-1}]$ and S_y [-] are specific storage and yeild, respectively, g $[\mathrm{m}\cdot\mathrm{s}^{-2}]$ is the gravitational constant and $\boldsymbol{g}$ $[\mathrm{m}\cdot\mathrm{s}^{-2}]$ is the gravitational vector, L [m] is a characteristic size of the yield layer, $\mathbb{K}$ $[\mathrm{m}^2]$ is an absolute permeability tensor, and Q $[\mathrm{kg}\cdot\mathrm{m}^{-3}\cdot\mathrm{s}^{-1}]$ is source or sink term.

It is common to see the Darcy Law written in terms of hydraulic head h and the hydraulic conductivity tensor $\mathbb{K}_h$:

$$\boldsymbol{q}_l = -\mathbb{K}_h \boldsymbol{\nabla} h, \tag{2.2a}$$

$$h = z + \frac{p_l}{\rho_l g}, \tag{2.2b}$$

$$\mathbb{K}_h = \mathbb{K}\frac{\rho_l g}{\mu_l}. \tag{2.2c}$$

2.2.3 Boundary conditions

Three types of *boundary conditions* are supported by the model:

1. prescribed pressure p_l (or head), see (2.3);
2. prescribed flux, i.e. normal component of the velocity $\boldsymbol{q}_l$, see (2.4);
3. semipervious boundary, see (2.5).

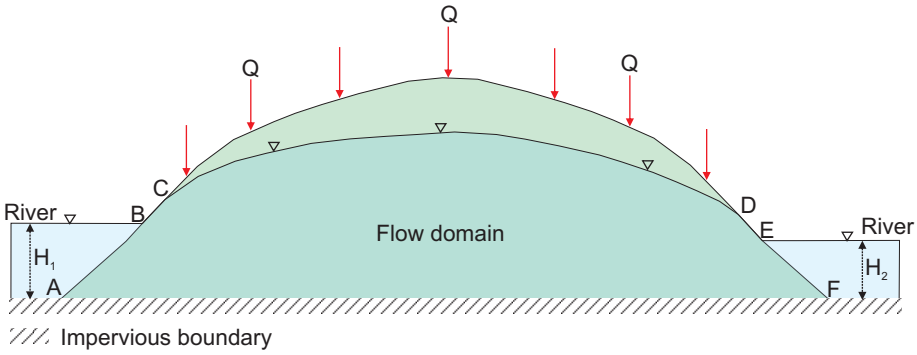

Figure 1: Flow domain between two rivers (Bear, 1972, it was partially based on).

Boundary of prescribed pressure or head. This involves the specification of a fixed pressure or hydrostatic head on boundary Γ_D. For instance, a boundary of this kind occurs whenever the flow domain is adjacent to a body of open water. Segments A-B and E-F in Fig. 1 are examples of a boundary of prescribed potential. The pressure or head boundary conditions are given functions, e.g.

$$p_l(\boldsymbol{x}, t) = p_b(\boldsymbol{x}, t), \quad \boldsymbol{x} \in \Gamma_D. \tag{2.3}$$

Boundary of prescribed flux. This involves the specification of the flux normal to the boundary Γ_N (see segment C-D in Figure 1):

$$\boldsymbol{q}_l \cdot \boldsymbol{n} = q_b(\boldsymbol{x}, t), \quad \boldsymbol{x} \in \Gamma_N, \tag{2.4}$$

where q_b $[\mathrm{m} \cdot \mathrm{s}^{-1}]$ is the given boundary flux. For infiltration at the top horizontal surface, it equals to the Darcy velocity and referred to as the infiltration velocity.

Semipervious boundary (or mixed boundary condition). This boundary condition is more complicated than the first two as it involves a case in which local conditions within the computational domain influence the flux in or out of the domain. This type of boundary occurs when the porous medium domain is in contact with a body of water continuum (or another porous medium domain, see for instance segments A-B and E-F in Fig. 1), however, a relatively thin semipervious layer separates the two domains:

$$\boldsymbol{q}_l \cdot \boldsymbol{n} = I \ \left(p(\boldsymbol{x}, t) - p_b(\boldsymbol{x}, t)\right), \quad \boldsymbol{x} \in \Gamma_R. \tag{2.5}$$

where I is an impedance and $p_b(\boldsymbol{x}, t)$ is the given external pressure.

2.3 Partially Saturated Flow

The Richards equation is often used to describe single phase flow under partially saturated conditions (i.e., the pores are not occupied exclusively by a single phase). As such, it requires the introduction of a relative permeability and a capillary pressure relations. The Richards equation is well suited to very large numerical problems (millions of degrees of freedom) because it requires only one independent variable per cell.

2.3.1 Assumptions and Applicability

The Richards equation makes the fundamental assumption that we are neglecting the movement of the gas phase. Because of this assumption, using the Richards equation may limit the kinds of transport analysis that can be done. It should also be noted that the Richards equation is often highly nonlinear due to strong dependence of the relative permeability of the liquid phase on the liquid saturation. We also assume that there are no fractures and the water flows through the pores only.

2.3.2 Process Model Equations

The Richards equation is derived from the conservation of liquid mass equation. In the mixed formulation it is written for the volumetirc water content θ $[\mathrm{mol}\cdot\mathrm{m}^{-3}]$ and the Darcy velocity $\boldsymbol{q}_l$ $[\mathrm{m}\cdot\mathrm{s}^{-1}]$:

$$\frac{\partial\theta(p_l)}{\partial t} = -\boldsymbol{\nabla}\cdot(\eta_l\boldsymbol{q}_l) + Q, \tag{2.6a}$$

$$\boldsymbol{q}_l = -\frac{\mathbb{K}k_{rl}}{\mu_l}(\boldsymbol{\nabla}p_l - \rho_l\boldsymbol{g}), \tag{2.6b}$$

where η_l $[\mathrm{mol}\cdot\mathrm{m}^{-3}]$ is the molar liquid density, Q $[\mathrm{kg}\cdot\mathrm{m}^{-3}\cdot\mathrm{s}^{-1}]$ is source or sink term, $\mathbb{K}$ $[\mathrm{m}^2]$ is absolute permeability tensor, μ_l $[\mathrm{Pa}\cdot\mathrm{s}\,]$ is liquid viscosity, ρ_l $[\mathrm{kg}\cdot\mathrm{m}^{-3}\,]$ is liquid density, and k_{rl} [-] is relative permeability. The total volumetric water content θ is defined as a product of porosity ϕ, molar liquid density η_l and liquid saturation s_l:

$$\theta(p_l) = \phi(p_l)\eta_l\, s_l(p_c).$$

Usage of the molar liquid density θ allows us to easily extend the model to a non-isothermal case.

Just like in the case of the fully saturated flow (2.1), the primary dependent variable in (2.6) is liquid pressure p_l. The difference with (2.1) is in that the pressure enters the equations in a nonlinear form, through a dependence $\theta_l(p_l)$ to be discussed in the following sections.

In general the porosity ϕ is a functions of pressure p_l. The relative permeability k_{rl} is a function of saturation s_l, which in turns is a function of capillary pressure p_c. The relation between pressures p_l and p_c will be discussed in the next section. Typical models of relative permeability are the van Genuchten-Mualem relations (2.17) and the Brooks-Corey-Burdine relations (2.19). The equation (2.6) is continuous when transitioning from the saturated to the vadoze zones.

2.3.3 Capillary Pressure – Saturation Relations

Richards equation for unsaturated flow requires representations of the capillary pressure p_c and the relative permeability k_{rl}. The capillary pressure is a fundamental dependent variable in the multiphase flow model, and relates the difference in pressure across an interface between two fluids to the tendency of a porous medium to pull in the wetting fluid and push out the non-wetting one. For the partially saturated fluid flow model typically used to characterize air-water systems, there is only a single capillary pressure:

$$p_c = p_g - p_l \tag{2.7}$$

where p_g is the pressure of the air/gas.

Let us define the effective liquid saturation s_e as

$$s_e \;=\; \frac{s_l - s_l^r}{s_l^0 - s_l^r}, \tag{2.8}$$

where s_l^0 is the maximum and s_l^r is the residual (i.e. minimum) liquid saturations. Notice that (2.8) implies the effective saturation s_e takes values in the range from zero to one.

Using these definitions, two widely used capillary pressure-saturation model relations are presented below, namely the Brooks-Corey (Brooks and Corey, 1964) and van Genuchten (van Genuchten, 1980) models.

Brooks-Corey model. The Brooks-Corey form of the saturation function (Brooks and Corey, 1964) is given by

$$s_e \;=\; (\alpha|p_c|)^{-\lambda}, \tag{2.9}$$

where the empirical parameters λ [-], and α [Pa^{-1}] are fit to experimental observations. The inverse relation is written as

$$p_c \;=\; \frac{1}{\alpha} s_e^{-1/\lambda}. \tag{2.10}$$

Van Genuchten model. In the van Genuchten (1980) model the effective liquid saturation is described by the relation

$$s_e \;=\; \left[1 + (\alpha|p_c|)^n\right]^{-m}, \tag{2.11}$$

with inverse relation

$$p_c \;=\; \frac{1}{\alpha}\left[s_e^{-1/m} - 1\right]^{1/n}. \tag{2.12}$$

The non-dimensional constants n [-], m [-] and dimensional α [Pa^{-1}] are empirical parameters.

One may notice that Van Genuchten model is an evolution of Brooks-Corey model as evident both by the dates and the form of the equations. In particular notice that if we take $\lambda = mn$ and $(\alpha p_c)^n \gg 1$, then the Brooks-Corey and van Genuchten saturation functions, Equations (2.9) and (2.11), are equivalent.

2.3.4 Relative Permeability – Saturation Relations

Given capillary pressure - saturation relations $p_c(s_l$, the relative permeability relations needed by Richards equation can be defined. Two popular relative permeability - saturation relations used in air-water systems are the Mualem (1976) and Burdine (1953) models. The relative permeability model proposed by Mualem (1976) has the form

$$k_{rl}(s_l) = s_e^{\ell} \frac{\left\{ \int_0^{s_e} p_c(s)^{-1} ds \right\}^2}{\left\{ \int_0^{1} p_c(s)^{-1} ds \right\}^2}, \tag{2.13}$$

where the power ℓ in s_e^{ℓ} is a pore-connectivity parameter that varies depending on the soil. Although, Mualem (1976) estimated an average value of $\ell = 1/2$, values of ℓ ranged from -5 to +5 across soils. More recent studies [cf. van Genuchten et al. (1991)] have suggested that $\ell = 1/2$ may be appropriate for coarse-textured soils, but not for many medium- and fine-textured soils. Thus, ℓ should be available as a fitting parameter.

Similarly, the older Burdine (1953) model is given by

$$k_{rl}(s_l) = s_e^{\ell} \frac{\int_0^{s_e} p_c(s)^{-2} ds}{\int_0^{1} p_c(s)^{-2} ds}, \tag{2.14}$$

where Burdine (1953) assumed $\ell = 2$. However, as with the Mualem model (2.13), ℓ, should be available as a fitting parameter.

Van Genuchten relative permeability. To obtain a closed-form solution for the relative permeability using either the Mualem or Burdine models (Eqns.(2.13) and (2.14), respectively) combined with the van Genuchten saturation function, the parameters n and m must be related by the expressions

$$m = \begin{cases} 1 - \dfrac{1}{n}, & \text{Mualem}, \\ 1 - \dfrac{2}{n}, & \text{Burdine}. \end{cases} \tag{2.15}$$

In the more general case of independent values of m and n the relative permeability involves the incomplete beta function (van Genuchten and Nielsen, 1985). More recently (Dourado Neto et al., 2011) presented a general model for Mualem and Burdine relative permeability functions for use with the van Genuchten saturation function in terms of hypergeometric functions.

The Burdine relative permeability function for the liquid phase derived from the van Genuchten saturation function is given by

$$k_{rl} \;=\; s_e^2 \left\{ 1 - \left[1 - s_e^{1/m} \right]^m \right\}. \tag{2.16}$$

The Mualem relative permeability function has the form (note power 2):

$$k_{rl} \;=\; s_e^{\ell} \left\{ 1 - \left[1 - s_e^{1/m} \right]^m \right\}^2. \tag{2.17}$$

Brooks-Corey relative permeability. Combined with the Brooks-Corey saturation function, the Mualem relative permeability function is given by

$$k_{rl} = \left(s_e\right)^{\ell+2+2/\lambda} = \left(\alpha|p_c|\right)^{-((\ell+2)\lambda+2)}. \tag{2.18}$$

The Burdine form originally considered by Brooks and Corey (1964) is given by

$$k_{rl} = \left(s_e\right)^{\ell+1+2/\lambda} = \left(\alpha|p_c|\right)^{-((\ell+1)\lambda+2)}. \tag{2.19}$$

2.3.5 Boundary conditions

To facilitate the discussion on boundary conditions, consider the case of flow described in Fig. 1. Although the figure represents a two-dimensional flow field, the passage to three dimensions is straightforward and requires no further explanations.

Four types of boundary conditions are supported by the model:

1. prescribed pressure p_l (or head), see (2.20);
2. prescribed flux, i.e. normal component of the velocity $\boldsymbol{q}_l$, see (2.21);
3. semipervious boundary, see (2.22);
4. seepage face.

Boundary of prescribed pressure or head. This involves the specification of a fixed pressure or hydrostatic head on boundary Γ_D. For instance, a boundary of this kind occurs whenever the flow domain is adjacent to a body of open water. Segments A-B and E-F in Fig. 1 are examples of a boundary of prescribed potential. The pressure or head boundary conditions are given functions, e.g.

$$p_l(\boldsymbol{x}, t) = p_b(\boldsymbol{x}, t), \quad \boldsymbol{x} \in \Gamma_D. \tag{2.20}$$

Boundary of prescribed flux. This involves the specification of the flux normal to the boundary Γ_N (see segment C-D in Figure 1):

$$\boldsymbol{q}_l \cdot \boldsymbol{n} = q_b(\boldsymbol{x}, t), \quad \boldsymbol{x} \in \Gamma_N, \tag{2.21}$$

where q_b $[\mathrm{m} \cdot \mathrm{s}^{-1}]$ is the given boundary flux. For infiltration at the top horizontal surface, it equals to the Darcy velocity and referred to as the infiltration velocity.

Semipervious boundary (or mixed boundary condition). This boundary condition is more complicated than the first two as it involves a case in which local conditions within the computational domain influence the flux in or out of the domain. This type of boundary occurs when the porous medium domain is in contact with a body of water continuum (or another porous medium domain, see for instance segments A-B and E-F in Fig. 1), however, a relatively thin semipervious layer separates the two domains:

$$\boldsymbol{q}_l \cdot \boldsymbol{n} = I \, \left(p(\boldsymbol{x}, t) - p_b(\boldsymbol{x}, t)\right), \quad \boldsymbol{x} \in \Gamma_R. \tag{2.22}$$

where I is an impedance and $p_b(\boldsymbol{x}, t)$ is the given external pressure.

Seepage face. As is shown in Fig. 1 (see segments B-C and D-E), seepage face (or surface) is always present when a phreatic surface ends at the down-stream external boundary of flow domain. In this case the phreatic surface is tangent to the boundary of the porous medium at points C and D. Along a seepage surface, water emerges from the flow domain, trickling downward to the adjacent body of water.

A seepage surface is defined as the boundary where water leaves the ground surface and then continues to flow in a thin film along its surface. Being exposed to the atmosphere, the pressure along the seepage face is equal to the atmospheric pressure (i.e. capillary pressure $p_c = 0$).

The geometry of the seepage face is known (as it coincides with the boundary of the porous medium), except for its limit (points C and D in Figure 1) which is also lying on the (a priori) unknown phreatic surface. The location of this point is, therefore, part of the required solution. In unsteady flow, the location of the upper limit of the seepage face varies with time and could be simulated in two ways:

1. Using a dynamic boundary condition that switches from a prescribed pressure boundary condition to a prescribed flux boundary condition representing the recharge.
2. Combining boundary conditions in a hybrid one to represent the transition recharge/seepage surface (e.g. see Fig. 2).

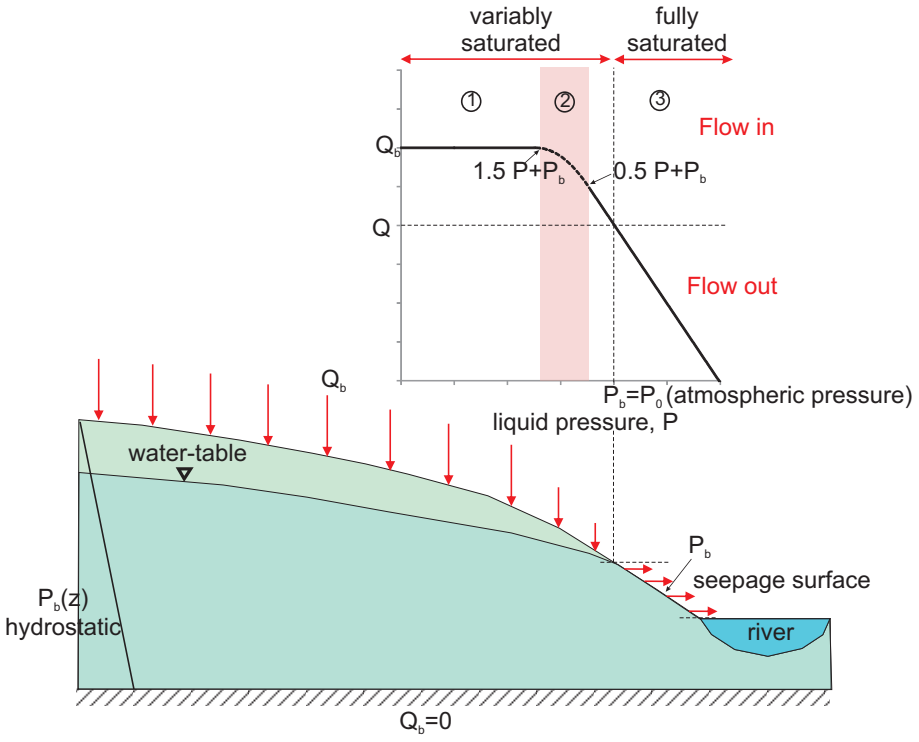

Figure 2: Seepage face.

The state of the first option depends on the pressure inside the computational domain. Regarding the second option, this hybrid boundary condition (based on Hamm and Aleman, 2000) can be

formulated as

$$\begin{aligned}
\boldsymbol{q}_l \cdot \boldsymbol{n} &= q_b(t) && \text{for} \quad p < \left(\tfrac{3}{2}p' + p_0\right), \\
\boldsymbol{q}_l \cdot \boldsymbol{n} &= \tfrac{\left(7-2f-f^2\right)}{8} q_b(t) && \text{for} \quad \left(\tfrac{3}{2}p' + p_0\right) \leq p \leq \left(\tfrac{1}{2}p' + p_0\right), \\
\boldsymbol{q}_l \cdot \boldsymbol{n} &= I(p - p_0) && \text{for} \quad \left(\tfrac{1}{2}p' + p_0\right) < p,
\end{aligned} \tag{2.23}$$

where $q_b(t)$ is the maximum recharge and $f(p,t)$ is a local variable between -1 and 1 defined as

$$f(p,t) = 2\frac{p' - (p(x_b, y_b, z_b, t) - p_0)}{p'}, \tag{2.24}$$

where p_0 is a reference pressure (in this particular example case, its value is equal to the atmospheric pressure), and p' is defined as

$$p' = I^{-1} q_b(t). \tag{2.25}$$

2.4 Isothermal Richards Equation with Dual Porosity Model

Dual porosity model is designed to model fluid flows when the solid contains both pores/matrix and fractures.

2.4.1 Assumptions and Applicability

Typically flow in the fracture is much faster that that in the pores/matrix. Therefore, dual-porosity model assumes that water flow is restricted to the fractures. The pores in the solid material (e.g. rock) represent immobile pockets that can exchange, retain and store water but do not permit convective flow. This leads to dual-porosity type flow and transport models that partition the liquid phase into mobile and immobile regions.

2.4.2 Process Model Equations

The Richards equation in the mobile (fracture dominated) region is augmented by the water exchange term Σ_w:

$$\frac{\partial \theta_f}{\partial t} = -\boldsymbol{\nabla} \cdot (\eta_l \boldsymbol{q}_l) + Q_f - \Sigma_w, \tag{2.26a}$$

$$\boldsymbol{q}_l = -\frac{\mathbb{K} k_r}{\mu}(\boldsymbol{\nabla} p_l - \rho_l \boldsymbol{g}), \tag{2.26b}$$

where Σ_w is the transfer rate of water from the matrix to the fracture, and Q_f is source or sink term $[\mathrm{kg} \cdot \mathrm{m}^{-3} \cdot \mathrm{s}^{-1}]$. The equation for water balance in the matrix is

$$\frac{\partial \theta_m}{\partial t} = Q_m + \Sigma_w,$$

where and Q_m is source or sink term $[\mathrm{kg} \cdot \mathrm{m}^{-3} \cdot \mathrm{s}^{-1}]$. The volumetric water contents θ_f and θ_m are defined as

$$\theta_f = \phi_f \, \eta_l \, s_{lf}, \qquad \theta_m = \phi_m \, \eta_l \, s_{lm},$$

where saturations s_{lf} and s_{lm} may use different capillary pressure-saturation models. The rate of water transfer from the matrix to the fracture regions Σ_w is proportional to the difference in hydraulic heads:

$$\Sigma_w = \alpha_w (h_f - h_m),$$

where α_w is the mass transfer coefficient. Since hydraulic heads are needed for both regions, this equation requires estimating retention curves for both regions and therefore is nonlinear.

2.4.3 Boundary conditions

To facilitate the discussion on boundary conditions, consider the case of flow described in Fig. 1. Although the figure represents a two-dimensional flow field, the passage to three dimensions is straightforward and requires no further explanations.

In the dual porosity model one has to specify the boundary conditions for the fracture and the matrix (pores). Due to the assumption that the pores do not permit convective flow,

the boundary conditions for the matrix are always zero flux conditions:

$$\boldsymbol{q}_m \cdot \boldsymbol{n} = 0, \quad \boldsymbol{x} \in \Gamma. \tag{2.27}$$

Boundary of prescribed pressure or head for fracture. This involves the specification of a fixed pressure or hydrostatic head on boundary Γ_D. For instance, a boundary of this kind occurs whenever the flow domain is adjacent to a body of open water. Segments A-B and E-F in Fig. 1 are examples of a boundary of prescribed potential. The pressure or head boundary conditions are given functions, e.g.

$$p_f(\boldsymbol{x}, t) = p_b(\boldsymbol{x}, t), \quad \boldsymbol{x} \in \Gamma_D. \tag{2.28}$$

Boundary of prescribed flux for fracture. This involves the specification of the flux normal to the boundary Γ_N (see segment C-D in Figure 1):

$$\boldsymbol{q}_f \cdot \boldsymbol{n} = q_b(\boldsymbol{x}, t), \quad \boldsymbol{x} \in \Gamma_N, \tag{2.29}$$

where q_b $[\mathrm{m} \cdot \mathrm{s}^{-1}]$ is the given boundary flux. For infiltration at the top horizontal surface, it equals to the Darcy velocity and referred to as the infiltration velocity.

Semipervious boundary (or mixed boundary condition). This boundary condition is more complicated than the first two as it involves a case in which local conditions within the computational domain influence the flux in or out of the domain. This type of boundary occurs when the porous medium domain is in contact with a body of water continuum (or another porous medium domain, see for instance segments A-B and E-F in Fig. 1), however, a relatively thin semipervious layer separates the two domains:

$$\boldsymbol{q}_f \cdot \boldsymbol{n} = I \, \left(p(\boldsymbol{x}, t) - p_b(\boldsymbol{x}, t)\right), \quad \boldsymbol{x} \in \Gamma_R. \tag{2.30}$$

where I is an impedance and $p_b(\boldsymbol{x}, t)$ is the given external pressure.

Seepage face. As is shown in Fig. 1 (see segments B-C and D-E), seepage face (or surface) is always present when a phreatic surface ends at the down-stream external boundary of flow domain. In this case the phreatic surface is tangent to the boundary of the porous medium at points C and D. Along a seepage surface, water emerges from the flow domain, trickling downward to the adjacent body of water.

A seepage surface is defined as the boundary where water leaves the ground surface and then continues to flow in a thin film along its surface. Being exposed to the atmosphere, the pressure along the seepage face is equal to the atmospheric pressure (i.e. capillary pressure $p_c = 0$).

The geometry of the seepage face is known (as it coincides with the boundary of the porous medium), except for its limit (points C and D in Figure 1) which is also lying on the (a priori) unknown phreatic surface. The location of this point is, therefore, part of the required solution. In unsteady flow, the location of the upper limit of the seepage face varies with time and could be simulated in two ways:

1. Using a dynamic boundary condition that switches from a prescribed pressure boundary condition to a prescribed flux boundary condition representing the recharge.

2. Combining boundary conditions in a hybrid one to represent the transition recharge/seepage surface (e.g. see Fig. 2).

The state of the first option depends on the pressure inside the computational domain. Regarding the second option, this hybrid boundary condition (based on Hamm and Aleman, 2000) can be formulated as

$$\begin{aligned} \boldsymbol{q}_f \cdot \boldsymbol{n} &= q_b(t) && \text{for} \quad p < \left(\tfrac{3}{2}p' + p_0\right), \\ \boldsymbol{q}_f \cdot \boldsymbol{n} &= \tfrac{\left(7-2f-f^2\right)}{8} q_b(t) && \text{for} \quad \left(\tfrac{3}{2}p' + p_0\right) \leq p \leq \left(\tfrac{1}{2}p' + p_0\right), \\ \boldsymbol{q}_f \cdot \boldsymbol{n} &= I(p - p_0) && \text{for} \quad \left(\tfrac{1}{2}p' + p_0\right) < p, \end{aligned} \tag{2.31}$$

where $q_b(t)$ is the maximum recharge and $f(p,t)$ is a local variable between -1 and 1 defined as

$$f(p,t) = 2\frac{p' - (p(x_b, y_b, z_b, t) - p_0)}{p'}, \tag{2.32}$$

where p_0 is a reference pressure (in this particular example case, its value is equal to the atmospheric pressure), and p' is defined as

$$p' = I^{-1} q_b(t). \tag{2.33}$$

3 Thermal Flow Processes

3.1 Overview

Heat flow and thermal conduction is an important aspect of many geochemical systems affecting chemical processes through changes in equilibrium and kinetic rate constants. Non-isothermal conditions can also result in buoyancy driven flow leading to convection cells and causing fingering phenomena due to differences in density.

Equations of state for fluid density, internal energy and/or enthalpy are needed in addition to heat capacity and thermal conductivity of the porous medium. Often the fluid properties for a complex mixture are unknown and the pure phase end member properties are used.

3.2 Model Equations

As heat flow is coupled to the Darcy flux, the heat equation itself is coupled to the flow equation as well as reactive transport equations through heat generated by chemical reactions. Conversely the flow and reactive transport equations are coupled to the heat equation through the temperature dependence of fluid properties such as density, viscosity, internal energy and enthalpy, and equilibrium thermodynamic and kinetic rate constants.

3.2.1 Partially saturated flow with water vapors

In the case of isothermal Richards equations it was possible to neglect water vapors, as presumably their concentration was the same everywhere. In the case when temperature variations cannot be neglected the effects of water vapors could be significant.

The Richards equation is derived from the conservation of liquid mass equation. Thus, changing vapor concentrations introduce an additional term

$$-\boldsymbol{\nabla} \cdot \left(\mathbb{K}_g \boldsymbol{\nabla} \frac{p_v}{p_g} \right)$$

into (2.6), where p_v and p_g [Pa] are the vapor and the gas pressures, respectively, and $\mathbb{K}_g$ is the effective diffusion coefficient of the water vapors. The gas pressure is presumed to be equal to the atmospheric one, while water vapor pressure is derived from the equilibrium of liquid and gas phases:

$$p_v = P_{\text{sat}}(T) \exp\left(\frac{P_{\text{cgl}}}{\eta_l R T} \right),$$

where P_{sat} is the saturated vapor pressure, P_{cgl} is the capilary gas-liquid pressure, and R is the ideal gas constant.

The Richards equation with gas vapors takes the form

$$\frac{\partial \theta(p_l)}{\partial t} = -\boldsymbol{\nabla} \cdot (\eta_l \boldsymbol{q}_l) - \boldsymbol{\nabla} \cdot \left(\mathbb{K}_g \boldsymbol{\nabla} \frac{p_v}{p_g} \right) + Q, \tag{3.1a}$$

$$\boldsymbol{q}_l = -\frac{\mathbb{K} k_{rl}}{\mu_l} (\boldsymbol{\nabla} p_l - \rho_l \boldsymbol{g}), \tag{3.1b}$$

where η_l is the molar liquid density, Q is source or sink term $[\mathrm{kg} \cdot \mathrm{m}^{-3} \cdot \mathrm{s}^{-1}]$, $\mathbb{K}$ is absolute permeability tensor, μ_l is liquid viscosity, ρ_l is liquid density, and k_{rl} is relative permeability. The total volumetric water content θ has to be modified to include the vapors

$$\theta = \phi \eta_l \, s_l + \phi (1 - \eta_l) X_l,$$

where X_l is molar fraction of water vapors.

The effective diffusion coeficient of water vapor is given by

$$\mathbb{K}_g = \phi g_g \tau_g \eta_g D_g,$$

where s_g is gas saturation, τ_g is the gas tortuosity, η_g is the molar density of gas, and D_g is the gas diffusion coefficient. The later, based on the TOUGHT2 model, is

$$D_g = D_{\text{ref}} \frac{P_{\text{ref}}}{p_g} \left(\frac{T}{T_{\text{ref}}} \right)^{\alpha},$$

where $D_{\text{ref}} = 2.14 \times 10^{-5}$, P_{ref} is the atmospheric pressure, $T_{\text{ref}} = 273.15$, $\alpha = 1.8$. Finally, we need a model for the gas tortuosity for which we use Millington and Quirk (1961) model

$$\tau_g = \phi^{\beta}, s_g^{\gamma}, \qquad \beta = 1/3, \quad \gamma = 7/3.$$

3.2.2 Energy Conservation Equation

The Richards equation with water vapor is coupled with the conservation of energy equation. One form of such equation in a porous medium with porosity ϕ is given by

$$\frac{\partial}{\partial t} \Big[\phi \rho_l u_l s_l + (1 - \phi) \rho_r u_r \Big] + \boldsymbol{\nabla} \cdot \left[-\frac{\mathbb{K} k_{rl}}{\mu_l} (\boldsymbol{\nabla} p_l - \rho_\alpha g \boldsymbol{e}_z) \rho_l h_l - Q_T \right] \; = \; Q_e, \tag{3.2}$$

where ρ_r and ρ_l are the density, u_r and u_l are the internal energy of the rock and the liquid phases, respectively; $\mathbb{K}$ is the absolute permeability tensor, k_{rl} is the relative permeability coefficient, s_l is the liquid saturation, μ_l is fluid viscosity, h_l is the enthalpy of the liquid phase, Q_T represents thermal conduction and radiation, and Q_e is a source or sink of energy. Note that the energy consumed/produced by chemical reactions is included in this last term.

The primary variables in (3.2) are the pressure p_l and the temperature T. The internal energies u_r and u_l are both functions of temperature. Assuming that the internal energy u_r and the thermal conduction Q_T have linear dependence on temperature,

$$u_r = c_r T \qquad \text{and} \qquad Q_T = \kappa T,$$

the equation (3.2) takes the form

$$\frac{\partial}{\partial t}\Big[\phi s_l \rho_l u_l + (1-\phi)\rho_r c_r T\Big] + \boldsymbol{\nabla}\cdot\Big[\boldsymbol{q}_l \rho_l h_l - \kappa \boldsymbol{\nabla} T\Big] \;=\; Q_e, \tag{3.3}$$

where T refers to temperature, $\boldsymbol{q}_l$ is the Darcy velocity

$$\boldsymbol{q}_l = -\frac{\mathbb{K} k_{rl}}{\mu_l}\left(\boldsymbol{\nabla} p_l - \rho_\alpha g \boldsymbol{e}_z\right), \tag{3.4}$$

the coefficient κ denotes the thermal conductivity of the medium and c_r refers to the specific heat of the porous medium. The internal energy and enthalpy are related by the equation

$$u_l \;=\; h_l - \frac{p_l}{\rho_l}. \tag{3.5}$$

Thermal conductivity if often described by the phenomenological relation given by Somerton et al. (1974)

$$\kappa \;=\; \kappa_{\rm dry} + \sqrt{s_l}(\kappa_{\rm sat} - \kappa_{\rm dry}), \tag{3.6}$$

where $\kappa_{\rm dry}$ and $\kappa_{\rm sat}$ are dry and fully saturated rock thermal conductivities, and s_l denotes the saturation state of the liquid.

Evapotranspiration. Evapotranspiration models should include all the processes that convert water from the aqueous phase into water in the gaseous phase, i.e., water vapor. This should also account for evaporation from soil and plant surfaces and plant transpiration and include options where these components vary wiith soil properties and structure of the plant canopy.

Equation of State. For multicomponent system, equation of state (EOS) data is required for water and all the NAPL components. Typically these are EOS for pure substances that are combined for mixtures. A basic EOS relates density to pressure and temperature. The form for the EOS is typically cubic such as the Soave-Redlich-Kwong (SRK) or the Peng-Robinson (PR) models. Tabular models are also in common use.

Mixture thermodynamics is used to combine pure phase EOS's for the application. The EPA lists over 80 potential NAPL components (volatile organic compounds or VOCs) that can cause groundwater contamination and has data bases with at least some properties for these contaminants.

Mixture Internal Energy and Enthalpy. These will generally follow the simple additive rule based of component values and mass fraction. Consideration must be also given to heats of solution.

3.3 Boundary Conditions

The boundary conditions for the thermal flow (3.1)-(3.2) consist of the conditions for each of the equations. The choice of the boundary conditions for (3.1) are identical to those of Isothermal

equaiton. We repeat those equations here for the sake of self-contained presentation. The boundary conditions for conservation of energy equation (3.2) may take the form of specified temperature or heat flux including zero temperature gradient. Initial conditions include specifying the temperature over the computational domain such as a constant value or derived from the geothermal gradient.

Specified temperature boundary conditions. These are Dirichlet type conditions on the temperature saying that at the boundary Γ_{TD}

$$T(\boldsymbol{x}, t) = T_b(\boldsymbol{x}, t), \quad \boldsymbol{x} \in \Gamma_{TD}, \tag{3.7}$$

where the temperature $T_b(\boldsymbol{x}, t)$ is given.

Specified heat flux boundary conditions. These are Neumann type boundary conditiosn on the temperature saying that at the boundary Γ_{TN}

$$\partial_{\boldsymbol{n}} T(\boldsymbol{x}, t) = \partial_{\boldsymbol{n}} T_b(\boldsymbol{x}, t), \quad \boldsymbol{x} \in \Gamma_{TD}, \tag{3.8}$$

where the temperature $\partial_{\boldsymbol{n}} T_b(\boldsymbol{x}, t)$ is given.

Boundary of prescribed pressure or head. This involves the specification of a fixed pressure or hydrostatic head on boundary Γ_{lD}. For instance, a boundary of this kind occurs whenever the flow domain is adjacent to a body of open water. Segments A-B and E-F in Fig. 1 are examples of a boundary of prescribed potential. The pressure or head boundary conditions are given functions, e.g.

$$p_l(\boldsymbol{x}, t) = p_b(\boldsymbol{x}, t), \quad \boldsymbol{x} \in \Gamma_{lD}. \tag{3.9}$$

Boundary of prescribed flux. This involves the specification of the flux normal to the boundary Γ_{lN} (see segment C-D in Figure 1):

$$\boldsymbol{q}_l \cdot \boldsymbol{n} = q_b(\boldsymbol{x}, t), \quad \boldsymbol{x} \in \Gamma_{lN}, \tag{3.10}$$

where q_b $[\mathrm{m} \cdot \mathrm{s}^{-1}]$ is the given boundary flux. For infiltration at the top horizontal surface, it equals to the Darcy velocity and referred to as the infiltration velocity.

Semipervious boundary (or mixed boundary condition). This boundary condition is more complicated than the first two as it involves a case in which local conditions within the computational domain influence the flux in or out of the domain. This type of boundary occurs when the porous medium domain is in contact with a body of water continuum (or another porous medium domain, see for instance segments A-B and E-F in Fig. 1), however, a relatively thin semipervious layer separates the two domains:

$$\boldsymbol{q}_l \cdot \boldsymbol{n} = I \, \left(p(\boldsymbol{x}, t) - p_b(\boldsymbol{x}, t) \right), \quad \boldsymbol{x} \in \Gamma_R. \tag{3.11}$$

where I is an impedance and $p_b(\boldsymbol{x}, t)$ is the given external pressure.

Seepage face. As is shown in Fig. 1 (see segments B-C and D-E), seepage face (or surface) is always present when a phreatic surface ends at the down-stream external boundary of flow domain. In this case the phreatic surface is tangent to the boundary of the porous medium at points C and D. Along a seepage surface, water emerges from the flow domain, trickling downward to the adjacent body of water.

A seepage surface is defined as the boundary where water leaves the ground surface and then continues to flow in a thin film along its surface. Being exposed to the atmosphere, the pressure along the seepage face is equal to the atmospheric pressure (i.e. capillary pressure $p_c = 0$).

The geometry of the seepage face is known (as it coincides with the boundary of the porous medium), except for its limit (points C and D in Figure 1) which is also lying on the (a priori) unknown phreatic surface. The location of this point is, therefore, part of the required solution.

4 Transport Processes

4.1 Overview

Transport is one of the most important process that needs to be accurately captured in the Environmental Management modeling tool set. In what follows, we use "Transport" to refer to the set of physical processes that lead to movement of dissolved and solid contaminants in the subsurface, treating the chemical reactions that can affect the transport rate through a retardation effect as a separate set of processes. The principal transport processes to be considered are *advection*, *mechanical dispersion*, and *molecular diffusion*. The equation for mass conservation of species C can be written as

$$\frac{\partial(\phi \sum_\alpha [s_\alpha C_{\alpha,i}])}{\partial t} + \boldsymbol{\nabla} \cdot \boldsymbol{J}_{\text{adv}} = \boldsymbol{\nabla} \cdot \boldsymbol{J}_{\text{disp}} + \boldsymbol{\nabla} \cdot \boldsymbol{J}_{\text{diff}} + Q,$$

where $C_{\alpha,i}$ is a concentration of ith species in phase α, $\boldsymbol{J}_{\text{adv}}$ is advective flux, $\boldsymbol{J}_{\text{disp}}$ is the dispersive flux, $\boldsymbol{J}_{\text{diff}}$ is the diffusive flux (often grouped with the dispersive flux), and Q is the summation of various source terms which may include reactions.

The principal assumptions associated with the transport process models derive from the continuum treatment of the porous medium. Pore scale processes, including the resolution of variations in transport rates within individual pores or pore networks (Kang et al., 2006; Li et al., 2008; Lichtner and Kang, 2007), are generally not resolved, although some capabilities for treating multi-scale effects are discussed in Section 4.3. In general, it is assumed that within any one Representative Elementary Volume (REV) corresponding to a grid cell all transport rates are the same. It will be possible, however, to define overlapping continua with distinct transport rates, as in the case where the fracture network and rock matrix are represented as separate continua.

Transport processes may be tightly coupled to both flow and reaction processes. In the case of flow, one important coupling is associated with the transport of chemical constituents that affect the density of the solution, which in turn affects flow rates through buoyancy. In the case of chemical reactions, the coupling effect is normally very strong for reactive constituents. Chemical reactions may consume components present in the gaseous phase (e.g., CO_2 or O_2), thus modifying the saturation of the phase itself. Reactions can strongly modify gradients, and thus transport rates, by either consuming or producing various chemical species.

4.2 Transport in Porous Medium

The name of this section indicates that we consider the pransport processes in the soil with pores, but no fractures. At the same time we still consider the gas and solid phases in addition to the liquid pahse.

4.2.1 Process Model Equations

The contaminants can be a part of one of three phases: solid, liquid or gas. When the contaminant i is present in the solid phase (e.g. ice) it is assumed not to be moving. One of the key assumptions of Richards equations used for flow models is that the gas phase is not moving. Therefore, the

concervation of mass equation in its general form (4.1) can be separated into equations for the liquid and gas phases. The equation for the species i dissolved in the liquid phase is

$$\frac{\partial(\phi s_l C_{l,i})}{\partial t} + \boldsymbol{\nabla} \cdot \boldsymbol{J}_{l,i}^{\text{adv}} = \boldsymbol{\nabla} \cdot \boldsymbol{J}_{l,i}^{\text{disp}} + \boldsymbol{\nabla} \cdot \boldsymbol{J}_{l,i}^{\text{diff}} + Q_{l,i} \tag{4.1}$$

and the equation for the pecies i in the gas phase is

$$\frac{\partial(\phi s_g C_{g,i})}{\partial t} = \boldsymbol{\nabla} \cdot \boldsymbol{J}_{g,i}^{\text{diff}} + Q_{g,i}. \tag{4.2}$$

The gas and liquid phases are related through an equation for saturations s_l and s_g

$$s_g = 1 - s_l.$$

The transition of the polutants between phases can be modeled through the source terms Q_*.

4.2.2 Assumptions and Applicability

We consider pure advection process and exclude the attenuation mechanisms and microbial behaviors that are discussed elsewhere. Note that there are situations where the advection could be modified by attributes of the transported mass and the pore structure. One is the potential for nonreactive anions to be repulsed by negatively charged solid surfaces into the center of pore throats where the velocity is faster. Another is the advection of inorganic and organic colloids, and microorganisms, whose movement can be affected by the geometry of pore throats. In addition to being subject to the same physicochemical phenomena as abiotic colloids, microorganisms have biological processes that can affect advection (e.g., temporal changes in surface properties due to changes in metabolic state; chemotaxis; predation).

4.2.3 Advective Fluxes

Advection is the process where the bulk fluid motion transports mass and heat. In the simplest conceptualization of advection, the mass of a component in a fluid parcel simply moves with the velocity of the fluid parcel. This assumes there are no other processes (e.g., diffusion, dispersion, reactions) that can affect the component concentration in the fluid parcel. Thus, advection can be a particulate or a dissolved species moving with the pore-water whose velocity is governed by the flow processes (discussed elsewhere). Continuum models have addressed these behaviors using bulk parameterizations to characterize the pore-scale controls and controlling chemical gradients.

Numerical difficulties with the accuracy, robustness, and computation efficiency of modeling the advection of moving steep concentration fronts, especially in complex velocity fields, are well known. In some cases, there are constraints on the Peclet and Courant numbers for the useful application of a given technique. The advective flux, $\boldsymbol{J}_{\text{adv}}$, of a dissolved species is described mathematically as

$$\boldsymbol{J}_{l,i}^{\text{adv}} = \phi s_l \boldsymbol{v}_l C_{l,i}, \tag{4.3}$$

where ϕ is the porosity, s_l is liquid saturation, $\boldsymbol{v}_l$ is the average linear velocity of the liquid, and $C_{l,i}$ is the concentration of the ith species in the liquid phase.

4.2.4 Dispersive Fluxes

Dispersion of a dissolved constituent refers to its spreading along tortuous pathways in a porous medium caused by mixing effects. Dispersion takes place in the direction of the flow (longitudinal) and normal to the flow (transverse). A conventional Eulerian Fickian representation of dispersion is assumed, which may be taken as the asymptotic limiting form of the dispersion tensor (Neuman, 1990). It should be noted that issues related to the scale dependence of dispersion are not considered. While this approach is known to have several limitations, such as backward dispersion against the direction of flow and scale independence, nevertheless, it is still widely used in practical applications. Furthermore, it may be the only approach for representing local scale dispersion.

The dispersive flux $\boldsymbol{J}_i^{\text{disp}}$ for a variably saturated porous medium has the form

$$\boldsymbol{J}_i^{\text{disp}} \;=\; -\phi s_\alpha \boldsymbol{D} \boldsymbol{\nabla} C_i, \tag{4.4}$$

described in analogy to a Fickian process, where $\boldsymbol{D}$ denotes the dispersion tensor. The dispersion tensor takes different forms depending on whether the media is isotropic or anisotropic.

Isotropic Media. For an isotropic medium with no preferred axis of symmetry the dispersion tensor $\boldsymbol{D}$ has the well-known form (Bear, 1972)

$$\boldsymbol{D} \;=\; \alpha_T v \boldsymbol{I} + (\alpha_L - \alpha_T)\frac{\boldsymbol{v}\boldsymbol{v}}{v}, \tag{4.5}$$

$$= \begin{pmatrix} \alpha_T v + (\alpha_L - \alpha_T)\dfrac{v_x^2}{v} & (\alpha_L - \alpha_T)\dfrac{v_x v_y}{v} & (\alpha_L - \alpha_T)\dfrac{v_x v_z}{v} \\ (\alpha_L - \alpha_T)\dfrac{v_y v_x}{v} & \alpha_T v + (\alpha_L - \alpha_T)\dfrac{v_y^2}{v} & (\alpha_L - \alpha_T)\dfrac{v_y v_z}{v} \\ (\alpha_L - \alpha_T)\dfrac{v_z v_x}{v} & (\alpha_L - \alpha_T)\dfrac{v_z v_y}{v} & \alpha_T v + (\alpha_L - \alpha_T)\dfrac{v_z^2}{v} \end{pmatrix}, \tag{4.6}$$

characterized by the two parameters α_L [m] and α_T [m] referred to the longitudinal and transverse dispersivity, respectively. The vector $\boldsymbol{v} = (v_x,\, v_y,\, v_z)$ [m/s] denotes the average pore velocity with magnitude v, and $\boldsymbol{I}$ is the identity matrix.

Anisotropic Media. The dispersion tensor for anisotropic media has not received much attention, However, it has been shown that in an axi-symmetric medium with axis of symmetry $\boldsymbol{\lambda}_s$, the dispersion tensor takes the general form (Lichtner et al., 2002)

$$\begin{aligned} \boldsymbol{D} \;=\; & \alpha_T^H v \boldsymbol{I} + \left[\alpha_L^H - \alpha_T^V + \cos^2\theta \left(\alpha_L^V - \alpha_L^H + \alpha_T^V - \alpha_T^H\right)\right] \frac{\boldsymbol{v}\boldsymbol{v}}{v} \\ & + \left(\alpha_T^V - \alpha_T^H\right) v \left[\boldsymbol{\lambda}_s\boldsymbol{\lambda}_s - \frac{\cos\theta}{v}\left(\boldsymbol{\lambda}_s\boldsymbol{v} + \boldsymbol{v}\boldsymbol{\lambda}_s\right)\right], \end{aligned} \tag{4.7}$$

where $\alpha_L^{H,V}$ and $\alpha_T^{H,V}$ refer to the longitudinal and transverse dispersivity in the horizontal and vertical directions, and θ denotes the angle between the axis of symmetry and the flow velocity.

4.2.5 Diffusive Fluxes

Molecular diffusion is often indistinguishable from mechanical dispersion as a process operating in porous media, and thus the two are often lumped together to form a hydrodynamic dispersion term. Unlike dispersion, however, there is no effect of flow direction, so the potential difficulties associated with mismatches between flow and grid coordinate direction do not arise. Molecular diffusion is an entropy-producing process in which the random motion of molecules causes spreading or homogenization of a concentration field. Atomistic representations of molecular diffusion capture this random motion, but continuum models of the kind considered here typically represent only the average behavior of the molecules. It is noteworthy, however, that atomistic and continuum models for molecular diffusion do agree if sufficiently long time scales with a sufficient number of molecules are considered (Bourg et al., 2008).

The principal distinctions in the treatment of molecular diffusion are between those based on Fick's Law, which states that the diffusive flux is linearly proportional to the concentration gradient, and multicomponent treatments that take into account the buildup of electrostatic forces as the individual charged species (ions) attempt to diffuse at their own rate. In addition, a full treatment of molecular diffusion involves calculating fluxes in terms of gradients in chemical potential rather than concentration (Steefel and Maher, 2009).

In addition to the complexities associated with chemical interactions, it is also necessary to account for the effects of the porous medium through which diffusion occurs. Corrections to the diffusive flux are often represented with a tortuosity (see Section 4.2.5 below) based on an upscaled constitutive law intended to capture the heterogeneous pore geometries. Since diffusion may be restricted or eliminated through narrow pore throats, the effective diffusivity for a specific ion may be quite different from its diffusivity in water alone. Capturing the multiscale nature of the pore structure and its effect on molecular diffusion remains a challenge.

General Formulation for Molecular Diffusion. The most rigorous and general expression for molecular diffusion is given by

$$\boldsymbol{J}_j^{\text{diff}} = -\sum_i L_{ji} \boldsymbol{\nabla} \frac{\mu_i}{T}, \tag{4.8}$$

where the L_{ji} are the phenomenological coefficients introduced in the theory of irreversible thermodynamics (Lasaga, 1998; Onsager, 1931; Prigogine, 1968) and μ_j is the chemical potential of the ith species. Here, the fluxes are linearly related to gradients in the chemical potentials of the solutes rather than to their concentrations as in Fick's Law that follows. The phenomenological coefficients, L_{ji}, can be linked back to measurable quantities by making use of the mobility as the "velocity" of a particle acted upon by a force, with the force in this case provided by the chemical potential rather than the concentration

$$\boldsymbol{J}_j^{\text{diff}} = -\boldsymbol{\nabla}(M_j C_j \mu_j), \tag{4.9}$$

where u_j is the mobility of the jth ion defined by

$$M_j = \frac{D_j}{RT}. \tag{4.10}$$

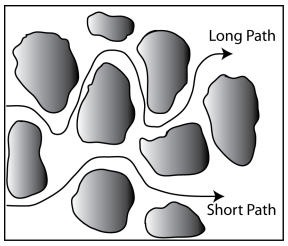

Figure 3: Tortuous diffusion paths in porous media (Steefel and Maher, 2009)

Single Species Diffusion (Fick's Law). Molecular diffusion is usually described in terms of Fick's First Law, which states that the diffusive flux is proportional to the concentration gradient

$$\boldsymbol{J}_i^{\text{diff}} \;=\; -\boldsymbol{\nabla}\left(D_i C_i\right). \tag{4.11}$$

D_i is referred to as the diffusion coefficient and is specific to the chemical component considered as indicated by the subscript i. Fick's First Law is a phenomenological theory for diffusion that relates diffusion to the "driving force" provided by the concentration gradient, although it can also be derived atomistically (Lasaga, 1998). In the case of diffusion in porous media, it is normally necessary to include a tortuosity correction as well (see discussion below).

Tortuosity. Since water-rock interaction commonly takes place in porous materials, it is important to account for the effect of tortuosity (Figure 3), which is defined as the ratio of the path length the solute would follow in water alone, L, relative to the tortuous path length it would follow in porous media, L_e (Bear, 1972)

$$\tau_L = \left(L/L_e\right)^2. \tag{4.12}$$

In this definition of tortuosity (sometimes the inverse of Equation (4.12) is used), its value is always less than one and the effective diffusion coefficient in porous media is obtained by multiplying the tortuosity by the diffusion coefficient for the solute in pure water.

With this formulation, the diffusion coefficient in porous media, D_i^*, is given by

$$D_i^* = \tau_L D_i. \tag{4.13}$$

The diffusive flux, then, is given by

$$\boldsymbol{J}_j^{\text{diff}} \;=\; -\boldsymbol{\nabla}\left(\phi s_\alpha D_j \tau_L C_j\right) \;=\; -\boldsymbol{\nabla}\left(\phi s_\alpha D_j^* C_j\right). \tag{4.14}$$

Various approaches for calculating formation factors (and thus, the diffusion coefficient in porous medium) are in use, with a formulation based on Archie's Law being the most common for fully saturated (single phase) systems

$$F_f \;=\; \frac{1}{a\phi^m}, \tag{4.15}$$

where a is a unitless fitting constant and m is unitless the cementation exponent.

For partially saturated systems, it is common to use the Millington-Quirk formulation (Millington and Quirk, 1961; Moldrup et al., 2000; Sumner, 2000)

$$D_i^* \;=\; \phi^{4/3} s_\alpha^{10/3} D_i, \tag{4.16}$$

where the saturation, s_α, can refer to either the gas or the aqueous phase.

4.2.6 Boundary Conditions

Boundary conditions have to be specified for each of the species concentrations C_i. A number of boundary conditions are possible for the diffusive flux, including a Dirichlet boundary conditions (prescribed concentration) and Neumann boundary conditions (prescribed flux).

Dirichlet Boundary Conditionis: These conditions specify a (typically fixed/constant) value of the concentration of the species, C_0, at the boundary location:

$$\boldsymbol{C}(\boldsymbol{x}) = \boldsymbol{C}_0. \tag{4.17}$$

Neumann Boundary Conditions: These conditions specify a value of the flux

$$\boldsymbol{J} \cdot \boldsymbol{n} = J_0^{\boldsymbol{n}}, \tag{4.18}$$

or concentration gradient

$$\frac{\partial \boldsymbol{C}}{\partial \boldsymbol{n}} = C_0^{\boldsymbol{n}}, \tag{4.19}$$

where either $J_0^{\boldsymbol{n}}$ or $C_0^{\boldsymbol{n}}$ is prescribed. The flux term can be a total, advective, or diffusive flux.

4.3 Single-Phase Transport with Dual Porosity Model

The multiscale nature of porous media and the transport processes associated is arguably the most significant and largely unresolved challenge for simulation of fate and transport in subsurface aquifers. Transport actually operates at the pore scale where variations in flow velocity and reaction rates can result in microscopic variability in transport rates. Continuum treatments of transport in porous media cannot resolve such sub-grid variations easily, although various upscaling techniques may be available for capturing the smaller scale behavior. In addition, multi-continuum or hybrid approaches may obviate the need for a formal upscaling procedure, although there are significant computational difficulties and expense associated with their implementation.

4.3.1 Process Model Equations

The dual porosity formulation of the solute transport consists of two equations for the fracture and matrix regions. In the fracture region, we have (Simunek and van Genuchten, 2008)

$$\frac{\partial(\phi_f s_{lf} C_f)}{\partial t} + \boldsymbol{\nabla} \cdot \boldsymbol{J}^{\text{adv}} = \boldsymbol{\nabla} \cdot \boldsymbol{J}^{\text{disp}} + \boldsymbol{\nabla} \cdot \boldsymbol{J}^{\text{diff}} - \Sigma_s + Q_f, \tag{4.20}$$

where s_{lf} is liquid saturation in fracture, Σ_s is the solute exchange term, and Q_f is source or sink term. In the matrix region, we have

$$\frac{\partial(\phi_m s_{lm} C_m)}{\partial t} = \Sigma_s + Q_m,$$

where s_{lm} is liquid saturation in matrix, Q_m is source or sink term. The solute exchange term is defined as

$$\Sigma_s = \alpha_s(C_f - C_m) + \Sigma_w C^*,$$

where C^* is equal to C_f if $\Sigma_w > 0$ and C_m if $\Sigma_w < 0$. The coefficient α_s is the first-order solute mass transfer coefficient [s^{-1}].

4.3.2 Boundary Conditions

For the dual porosity model boundary conditions have to be specified for the fracture and the matrix concentrations. The choice of the boundary conditions for the fracture component C_f are (4.21)-(4.23). Yet, we repeat them here for ease of reference. The boundary conditions for the matrix/pore component C_m are limited only to (4.21) and (4.23), and exclude the condition (4.22) on the flux values.

Boundary conditions have to be specified for each of the species concentrations C_i. A number of boundary conditions are possible for the diffusive flux, including a Dirichlet boundary conditions (prescribed concentration) and Neumann boundary conditions (prescribed flux).

Dirichlet Boundary Conditionis: These conditions specify a (typically fixed/constant) value of the concentration of the species, C_0, at the boundary location:

$$\boldsymbol{C}(\boldsymbol{x}) = \boldsymbol{C}_0. \tag{4.21}$$

Neumann Boundary Conditions: These conditions specify a value of the flux

$$\boldsymbol{J} \cdot \boldsymbol{n} = J_0^{\boldsymbol{n}}, \tag{4.22}$$

or concentration gradient

$$\frac{\partial \boldsymbol{C}}{\partial \boldsymbol{n}} = C_0^{\boldsymbol{n}}, \tag{4.23}$$

where either $J_0^{\boldsymbol{n}}$ or $C_0^{\boldsymbol{n}}$ is prescribed. The flux term can be a total, advective, or diffusive flux.

4.4 Data Needs

For modeling of molecular diffusion in porous media, two kinds of data are needed:

1. Experimental data on the diffusivities of individual ions in aqueous solution;
2. Characterization of the tortuosity of the porous medium under consideration. The tortuosity of the medium may be determined by a number of methods, including transport experiments involving tracers (Navarre-Sitchler et al., 2009), and microscopic imaging of the porous medium using synchrotron X-ray or related methods (Navarre-Sitchler et al., 2009), or estimation based on grain size and mineralogy of the materials. In addition, it may be possible to determine tortuosity from effective diffusion coefficients determined in field-scale experiments.

For the diffusivities of individual ions, there are some compilations in the literature (Lasaga, 1998; Steefel and Maher, 2009). While the diffusivity of individual ions could in theory be calibrated from field tests, normally they should be determined independently so that a more accurate determination of the tortuosity can be carried out.

5 Biogeochemical Reaction Processes

A range of biogeochemical reaction processes may be included in the HPC Simulator, including multicomponent aqueous complexation, sorption (including simple linear distribution coefficient, or Kd, and more complex multicomponent and multisite surface complexation and ion exchange models), mineral dissolution and precipitation, and microbially-mediated reactions.

5.1 Aqueous Complexation

5.1.1 Overview

It is customary to treat the reaction network corresponding to the homogeneous reactions in the aqueous phase as a distinct set of processes taking place within a single aqueous phase (Steefel and MacQuarrie, 1996). This reaction network is sometimes referred to as *aqueous complexation*, since it involves reactions between individual dissolved species to form complexes.

5.1.2 Process Model Equations

Equilibrium Reactions. If we assume that the various aqueous species are in chemical equilibrium, it is possible to reduce the number of *independent* concentrations, that is, the number that actually need to be solved for. Mathematically, this means that in a system containing N_{tot} aqueous species, the number of independent chemical components in the system N_c is reduced from the total number of species by the N_x linearly independent chemical reactions between them (for further discussion, see Aris (1965); Bowen (1968); Hooyman (1961); Kirkner and Reeves (1988); Lichtner (1985); Reed (1982); Van Zeggeren and Storey (1970). This leads to a natural partitioning of the system into N_c *primary* or *basis* species, designated here as C_j, and the N_x *secondary* species, referred to as C_i (Kirkner and Reeves, 1988; Lichtner, 1985; Reed, 1982). The equilibrium chemical reactions between the primary and secondary species take the form

$$\mathcal{A}_i \rightleftharpoons \sum_{j=1}^{N_c} \nu_{ij}\mathcal{A}_j \quad (i = 1, ..., N_x), \tag{5.1}$$

where $\mathcal{A}_j$ and $\mathcal{A}_i$ are the chemical formulas of the primary and secondary species respectively and ν_{ij} is the number of moles of primary species j in one mole of secondary species i. It should be noted here that the partitioning between the primary and secondary species is not unique, that is, we can write the chemical reactions in more than one way. The equilibrium reactions provide an algebraic link between the primary and secondary species via the law of mass action for each reaction

$$C_i = K_i^{-1}\gamma_i^{-1}\prod_{j=1}^{N_c}(\gamma_j C_j)^{\nu_{ij}} \quad (i = 1, ..., N_x), \tag{5.2}$$

where γ_j and γ_i are the activity coefficients for the primary and secondary species respectively, and K_i is the equilibrium constant of the reaction given in Equation (5.2), written here as the destruction of one mole of the secondary species. Equation (5.2) implies that the rate of production

of a primary component j due to homogeneous reactions, R_j^{aq}, can be written in terms of the sum of the total rates of production of the secondary species (Kirkner and Reeves, 1988)

$$R_j^{aq} \;=\; -\sum_{i=1}^{N_x} \nu_{ij} I_i^{aq}, \tag{5.3}$$

where I_i^{aq} is the reaction rate of the secondary species in the aqueous phase. Equation (5.3) suggests that one can think of a mineral dissolving, for example, as producing *only primary species* which then equilibrate instantly with the secondary species in the system. Using Equation (5.3) and neglecting transport for the sake of simplicity here, the rates of the equilibrium reactions can be eliminated (Steefel and MacQuarrie, 1996)

$$\frac{\partial}{\partial t}\left[\phi s_w \rho_w \left(C_j + \sum_{i=1}^{N_x} \nu_{ij} C_i\right)\right] = R_j^{min} \quad (j = 1, ..., N_c), \tag{5.4}$$

where s_w and ρ_w refer to the saturation and mass density of the aqueous phase, respectively. Note that only the term R_j^{min} remains on the right hand side of Equation (5.4) because we have assumed that they are the only kinetic reactions.

Definition of a Total Concentration. If a total concentration, Ψ_j, is defined as (Kirkner and Reeves, 1988; Lichtner, 1985; Reed, 1982)

$$\Psi_j = C_j + \sum_{i=1}^{N_x} \nu_{ij} C_i, \tag{5.5}$$

then the governing differential equations can be written in terms of the total concentrations in the case where only aqueous (and therefore mobile) species are involved (Kirkner and Reeves, 1988)

$$\frac{\partial}{\partial t}\left(\phi s_w \rho_w \Psi_j\right) + \boldsymbol{\nabla} \cdot \left[\phi s_w \rho_w \boldsymbol{v}_w \Psi_j - D \boldsymbol{\nabla}\left(\phi s_w \rho_w \Psi_j\right)\right] \;=\; R_j^{min} \quad (j = 1, ..., N_c), \tag{5.6}$$

where $\boldsymbol{v}_w$ is the velocity of the aqueous phase and $R_j^{\min}$ denotes the kinetic mineral reaction rate. As pointed out by Reed (1982) and Lichtner (1985), the total concentrations can usually be interpreted in a straightforward fashion as the total elemental concentrations (e.g., total aluminum in solution), but in the case of H^+ and redox species, the total concentration has no simple physical meaning and the total concentrations may take on negative values. Such quantities, however, do appear occasionally in geochemistry, the best example of which is alkalinity. In fact, the alkalinity (which may take on negative values) is just the negative of the total H^+ concentration where CO_2(aq) or $H_2\,CO_3$ is chosen as the basis species for the carbonate system.

Note that the total concentration is generally only a useful concept computationally where equilibrium reactions allow the definition of secondary species described with Equation (5.3). In the case where the reactions among aqueous species are described kinetically, then the various aqueous complexes cannot be eliminated algebraically and they have to be solved for individually.

Kinetic Aqueous Reactions. If the aqueous phase reactions are not sufficiently fast for a given time scale of interest that they reach equilibrium, then they must be treated kinetically by solving an ordinary differential equation. A convenient way to represent the reactions is with a Transition State Theory (TST) type of rate law (Aagaard and Helgeson, 1982; Lasaga, 1981, 1984)

$$I_j^{aq} \;=\; k_+^{aq}\left(\frac{Q^{aq}}{K^{aq}}\right)\prod a_i^n, \tag{5.7}$$

where k_+^{aq} is the rate constant for the aqueous reaction, Q^{aq} is the ion activity product , K^{aq} is the corresponding equilibrium constant, and a_i are the activities of the species affecting the rate far from equilibrium raised to the power n.

Alternatively, the reactions can be considered as completely irreversible, in which case there is no back reaction. A good example is radioactive decay. The reactions are assumed to take the form

$$I_j^{aq} \;=\; k_+^{aq}\prod a_i^n, \tag{5.8}$$

and are therefore similar to the TST form except that a dependence on the saturation state is missing. This more general form of irreversible reactions can be used to model decay and ingrowth of daughter products.

5.2 Aqueous Activity Coefficients

5.2.1 Overview

This Toolset includes models for thermodynamic activity coefficients in aqueous solutions. Multiple models, each with its own set of parameters and limitations, will be provided. In general, the toolset user must choose one such model to use in a given modeling application. In setting up to run the application, the user must ensure that a matching database with the requisite model-specific parameters is provided to support the run.

A key solution parameter associated with aqueous species activity coefficients is the ionic strength, defined as

$$\bar{I} \;=\; \frac{1}{2}\sum_i m_i z_i^2. \tag{5.9}$$

Here m_i denotes the molal concentration (molality) of the i^{th} solute species and z_i denotes its electrical charge number. Activity coefficients of charged solute species include a functional dependence on the ionic strength. The exact nature of this dependence depends on the specific model.

Activity coefficient models can be classified as to the upper limit of ionic strength to which a given model provides generally satisfactory results. For the most part, there are two kinds of such models. Low ionic strength models are generally usable up to an ionic strength of more or less 1 molal. Examples include the Davies equation and the B-dot equation. These models are based on simple equations and have a relatively small number of associated parameters. High ionic strength models are usable to very high ionic strength (>20 molal). The highest values of ionic strength normally seen are limited by the solubilities of highly soluble salts, such as calcium chloride and calcium nitrate. Examples of high ionic strength models include Pitzer's equations and Extended

UNIQUAC. High ionic strength models have more complex equations and require substantially more parameters than low ionic strength models. They are most likely to be applied to problems in which the ionic strength is higher than 1 molal. At low ionic strength, it is generally preferable to use a low ionic strength model, because the number of required parameters is smaller. In many instances, there will be sufficient supporting data available to support the use of low ionic strength models for large numbers of chemical components and species, but that may not be the case for the high ionic strength models. There are activity coefficient models that extend to intermediate ionic strength (4-6 molal). The NEA SIT model is an example. These models tend to be intermediate in equation complexity and number of required parameters. They have not received much attention to date in modeling geochemically complex systems.

It is noted that low ionic strength models are sufficient for many EM applications. Hanford tanks and the WIPP site pose notable exceptions, requiring the use of high ionic strength models. There may be other instances in which the use of low ionic strength models may be inappropriate.

There are two kinds of activity coefficients that a model should be able to provide. The first is the molal activity coefficient of a solute species (denoted by γ_i). This is subsequently used to compute the thermodynamic activity of the corresponding species (denoted by a_i). The activity of a species is obtained by multiplying the molality (molal concentration) of the species (denoted by m_i) by the molal activity coefficient:

$$a_i = m_i \gamma_i. \tag{5.10}$$

This activity is then used in various equations describing thermodynamic equilibrium and chemical kinetics.

The second kind of activity coefficient, the rational activity coefficient, pertains to the solvent, water (w). Its activity coefficient is denoted by λ_w to emphasize that it is different in kind: it is a mole fraction activity coefficient. The thermodynamic activity of water (a_w) is obtained by multiplying the mole fraction of water (X_w) by the activity coefficient of water:

$$a_w \ = \ X_w \lambda_w. \tag{5.11}$$

The activity of water is also different in kind from the activity of a solute species (a mole fraction activity as opposed to a molal activity). In treating the thermodynamics of aqueous electrolyte solutions, the activity of water and the activity of a solute species are almost always treated as described above.

Activity coefficients are generally first calculated in logarithmic form (e.g., $\ln \gamma_i$ or $\log \gamma_i$). In practical usage, activity coefficients are used most often used in base-10 logarithmic form, being converted from natural logarithm form as necessary. The conversion is illustrated by

$$\log \gamma_i = \frac{\ln \gamma_i}{\ln(10)}. \tag{5.12}$$

The conversion factor $\ln(10)$ is approximately equal to 2.303, and this value often appears in equations in the literature in place of the exact factor. The approximate value should not be used in this toolset, as it is insufficiently precise for accurate work. Instead the value should be calculated using the same floating-point precision that will be used to calculate activity coefficients. This is most efficiently done by calculating the value once and then storing it for subsequent use. It is noted

that "log" is somewhat ambiguous, in that the literature contains examples of it being used for both natural and base-10 logarithms. In the present description given in this section (Section 5.2), it will always refer to the base-10 logarithm.

Activity coefficient model equations ideally satisfy thermodynamic consistency relations. The value of consistency lies in allowing the possibility of accuracy at higher ionic strengths. Low ionic strength models typically include inconsistent equations, but the numerical consequences of the inconsistencies tend to be acceptable in the range of applicability of these models. For electrolyte solutions, Wolery (1992b) presents equations and methods for ensuring the development of consistent equations and for testing the consistency of existing sets of equations. The easiest means of testing for consistency is to use the cross-differentiation rule, which takes the following forms for solute-solute and solvent-solute pairs:

$$\frac{\partial \ln \gamma_j}{\partial m_i} = \frac{\partial \ln \gamma_i}{\partial m_j}, \tag{5.13}$$

$$N_w^{kg} \frac{\partial \ln a_w}{\partial m_i} = -1 - \sum_j m_j \frac{\partial \ln \gamma_i}{\partial m_j} \tag{5.14}$$

where i and j denote different solute species and N_w^{kg} is the number of moles of water in a 1 kg mass (approximately 55.51).

5.2.2 The Debye-Hückel Equations

Activity coefficient model equations for electrolyte solutions generally include some type of Debye-Hückel term to represent the effects of long-range electrical forces. The most common representation is based on the "extended" Debye-Hückel equation, which for the activity coefficient of an ionic solute species is given by

$$\log \gamma_i = -A_{\gamma,10} z_i^2 \left(\frac{\sqrt{\bar{I}}}{1 + b\sqrt{\bar{I}}} \right). \tag{5.15}$$

Here $A_{\gamma,10}$ is the Debye-Hückel "A" parameter for the activity coefficient (hence the subscript "γ"), modified for consistency with the base-10 logarithmic activity coefficient on the left-hand-side of the equation (hence the additional subscript, "10"). To assist in avoiding potential confusion, $A_{\gamma,10}$ should have a value of 0.5114 at 25°C and 1.013 bar pressure. The parameter "b" is conceptually the product of the Debye-Hückel "B" parameter for the activity coefficient (B_γ) and a length that corresponds to either the diameter of the ion in question or a characteristic distance of closest approach to itself or any other ion in solution. Practical models treat this in various ways. Some assign a constant value, typically 1.0, 1.2, or 1.5. Others use the product of B_γ (which has a known temperature and pressure dependence) and some sort of length parameter.

The equation for the activity of water corresponding to the extended Debye-Hückel equation is

$$\log a_w = \frac{1}{N_w^{kg}} \left(-\frac{\sum_i m_i}{\ln(10)} + \frac{2}{3} A_{\gamma,10} \bar{I}^{3/2} \varsigma(b\sqrt{\bar{I}}) \right). \tag{5.16}$$

where the summation over molalities spans all solute species (all aqueous species except the solvent), and the function ς(x) in Equation (5.16) is given by

$$\varsigma(x) \;=\; \frac{3}{x^3}\left(1+x-\frac{1}{1+x}-2\ln(1+x)\right), \tag{5.17}$$

where x serves the purpose of a generic variable. If the activity coefficient of water is desired, it can be obtained from the relation

$$\log \lambda_w \;=\; \log a_w - \log(X_w), \tag{5.18}$$

where the mole fraction of water is given by

$$X_w \;=\; \frac{N_w^{kg}}{N_w^{kg}+\sum_i m_i}. \tag{5.19}$$

The activity of water is closely related to the osmotic coefficient, φ:

$$\varphi \;=\; -\left(\frac{N_w^{kg}}{\sum_i m_i}\right)\ln a_w. \tag{5.20}$$

All forms of the extended Debye-Hückel equation are consistent with the Debye-Hückel Limiting Law (DHLL):

$$\lim_{\bar{I}\to 0}\log\gamma_i \;=\; -A_{\gamma,10}z_i^2\sqrt{\bar{I}}. \tag{5.21}$$

The limiting law is a critical feature describing the behavior of ionic activity coefficients in the range of very low ionic strength. The ionic activity coefficient plunges rapidly from unity as ionic strength increases from zero. There is no comparable limiting relation for the activity of water, due to the compositional dependence on both the ionic strength and the sum of solute molalities.

In general, the extended Debye-Hückel equation is not useful for significant practical modeling, as it is accurate only in very dilute aqueous solutions. If only monovalent ions are present, it may be useful for $\bar{I} < 0.1$ molal. In the presence of higher valence ions, the maximum range becomes more compressed. Most practical models therefore extend the "extended" Debye-Hückel equation by adding additional terms or otherwise adding to the mathematical complexity, in the process introducing more model parameters.

The activity coefficient models that will be available in this toolset include the Davies equation, the B-dot equation, Pitzer's equations, Extended UNIQUAC, and NEA-SIT. The models are first addressed, followed by the discussion on rescaling the activity coefficients.

5.2.3 The Davies Equation

The Davies (1962) equation is a commonly used at low ionic strength (less than about 1 molal) model. The activity coefficient of an aqueous solute species is given by

$$\log\gamma_i \;=\; -A_{\gamma,10}z_i^2\left(\frac{\sqrt{\bar{I}}}{1+\sqrt{\bar{I}}}-d\bar{I}\right). \tag{5.22}$$

Here d is a constant, either 0.2 as in EQ3/6 (Wolery, 1992a) or 0.3 as in PHREEQC (Parkhurst and Appelo, 1999). If the "$d\bar{I}$" part is dropped, this equation reduces to the extended Debye-Hückel form with b set to unity. It can be shown that the full equation satisfies the solute-solute-form of the cross-differentiation rule.

For the activity coefficient of water, the matching equation used in EQ3/6 for the activity of water is

$$\log a_w \;=\; \frac{1}{N_w^{kg}} \left(-\frac{\sum_i m_i}{\ln(10)} + \frac{2}{3} A_{\gamma,10} \bar{I}^{\frac{3}{2}} \varsigma(\sqrt{\bar{I}}) - d A_{\gamma,10} \bar{I}^2 \right). \tag{5.23}$$

where all parameters and the $\varsigma(x)$ function have been previously introduced (See Section 5.2.2). This equation is a corrected version of that given by Wolery (1992a) (Equation 86 in that document). Here a factor of 2 in the "*d*" term has been removed, and d substitutes for the original constant value of 0.2. This equation is quasi-consistent with the equation for the activity coefficient of a solution species, in the sense that the solvent-solute form of the cross-differentiation rule is satisfied for the case of a pure solution of a uni-univalent electrolyte, such as sodium chloride. It does not satisfy this rule in the general case.

The equation used by PHREEQC is symbolically equivalent to

$$a_w \;=\; 1 - \frac{1}{N_w^{kg}} \sum_i m_i. \tag{5.24}$$

As given by the source (Parkhurst and Appelo, 1999, p. 17), the factor $1/N_w^{kg}$ is replaced by a constant value of 0.017, which is rather approximate, and the molality is replaced by the mole number divided by the number of kg of solvent water (this substitution is exact). This equation is based on ignoring the activity coefficient of water and replacing the mole fraction with a limiting approximation of itself. Hence, the activity of water is given in direct form, rather than logarithmically.

For the present toolset, it is recommended that the Davies model be implemented as two options, one (Davies-EQ3/6) consistent with the implementation in EQ3/6, the other (Davies-PHREEQC), with PHREEQC. This will permit direct comparison with both codes.

The Davies equation predicts a unit activity coefficient for electrically neutral solute species. This is known to be generally inaccurate, as the activity coefficients of non-polar neutral solutes such as O_2(aq) and N_2(aq) should increase with ionic strength (the "salting out" effect), while the activity coefficients of polar species such as $CaSO_4$(aq) and $MgSO_4$(aq) should decrease ("salting-in").

In practice, the Davies equation is mainly used for low temperatures (near 25°C) and near-atmospheric pressures. The $A_{\gamma,10}$ parameter has temperature and pressure dependence. As long as this is accounted for, the Davies equation model could be applied in principle at higher temperatures and pressures. However, it needs to be kept in mind that the 0.2 constant was obtained by fitting data to solutions for temperature near 25°C and for atmospheric pressure. The accuracy of the model is therefore likely to deteriorate at higher temperatures and pressures.

5.2.4 The B-dot Equation

The B-dot equation of Wolery (1969) is an alternative low ionic strength model. The activity coefficient of a solute species is given by

$$\log \gamma_i \;=\; -\frac{A_{\gamma,10} z_i^2 \sqrt{\bar{I}}}{1 + \mathring{a}_i B_\gamma \sqrt{\bar{I}}} + \dot{B}\bar{I}. \tag{5.25}$$

where $\mathring{a}_i$ is the diameter of the i^{th} solute species, B_γ is the Debye-Hückel B parameter for the activity coefficient, and $\dot{B}$ is the "B-dot" parameter. Removing the $\dot{B}\bar{I}$ term and setting $\mathring{a}B_\gamma$ to unity, this equation reduces to the Davies equation with the $d\bar{I}$ term omitted. Comparison with the Davies equation brings up two points. The first is that the B-dot model has more parameters. The B_γ parameter appears, and each solute species has an assigned diameter. The "B-dot" parameter itself is an additional parameter.

It can be shown that the B-dot equation does not satisfy the solute-solute form of the cross-differentiation rule. There is an issue with the first term on the right hand side in that the rule can only be satisfied if all aqueous ions have the same diameter. There is an issue with the second term in that the rule is only satisfied if the charge number squared is the same for all ions, as would be the case for example in a pure sodium chloride solution.

For an electrically neutral species, the B-dot equation reduces to

$$\log \gamma_i \;=\; \dot{B}\bar{I}. \tag{5.26}$$

As the $\dot{B}$ parameter is generally assigned a positive value, this would provide for some measure of "salting-out." By tradition, however, the B-dot equation is not applied to neutral solute species, and it will not be so applied in the present toolset. For non-polar neutral species, the common practice is to assign an approximation for the activity coefficient of CO_2(aq) in otherwise pure sodium chloride solution of the same ionic strength. The approximation used in EQ3/6 (based on S. E. Drummond (1981), and which will be adopted for the present toolset) is

$$\ln \gamma_i \;=\; \left(C + FT + \frac{G}{T}\right) I - (E + HT)\left(\frac{\bar{I}}{\bar{I} + 1}\right). \tag{5.27}$$

Here T is the absolute temperature and C = -1.0312, F = 0.0012806, G = 255.9, E = 0.4445, and H = -0.001606. Note that the result is presented in terms of the natural logarithm. For a polar aqueous species, the EQ3/6 practice (which will be adopted in the present toolset) is to use

$$\log \gamma_i \;=\; 0. \tag{5.28}$$

Because different equations are used for electrically neutral solute species than for ionic species, there is necessarily an additional set of violations of the solute-solute cross-differentiation rule.

For the activity of water, the B-dot model as implemented in EQ3/6 (and recommended for the present toolset) is to use the equation

$$\log a_w = \frac{1}{N_w^{kg}}\left(-\frac{\sum_i m_i}{\ln(10)} + \frac{2}{3} A_{\gamma,10} \bar{I}^{\frac{3}{2}} \sigma(\mathring{a}B_\gamma \sqrt{\bar{I}}) - \dot{B}\bar{I}^2\right). \tag{5.29}$$

All the parameters here have been introduced previously, except for the unsubscripted $\mathring{a}$, which is conceptually an effective solute species diameter. In practice, this is assigned a constant value of 4.0 angstroms.

The above equation for the activity of water is quasi-consistent with the solvent-solute form of the cross-differentiation rule. The term containing the effective solute diameter leads to inconsistency unless every ionic solute has a matching diameter value. The term containing $\dot{B}$ leads to inconsistency unless the solution is a pure solution of a uni-univalent electrolyte such as sodium chloride.

The thermodynamic inconsistencies noted above introduce some level of inaccuracy into the model, tending to negate the improvement that might be expected by introducing more parameters (e.g., a diameter value specific to each solute species). Thus, for temperature near 25°C and near-atmospheric pressure, the B-dot model is probably as good as the Davies equation model.

The B-dot model does have an advantage over the Davies equation model in that it is better parameterized to cover a wide range of temperature and pressure. In addition to $A_{\gamma,10}$, the $B_\gamma$and $\dot{B}$ parameters are treated as functions of temperature and pressure. The $A_{\gamma,10}$ and B_γ parameters have values derived from pure theory (and models for pure water properties). The $\dot{B}$ parameter is obtained by fitting to data for pure sodium chloride solutions. The ion size parameters are treated as constant with respect to temperature and pressure.

In regard to solute species, diameters are only necessary for ionic species. Some means needs to be provided to specify (as on a supporting thermodynamic data file) whether a neutral species is to be treated as non-polar or polar. All the necessary information could be folded into a diameter array or equivalent structure, in which the values in the case of neutral species would not be actual diameters, but code values specifying non-polar or polar type. However, a separate flagging structure should be utilized, as the variable type can then be something more appropriate (integer or logical) than the floating point necessary for actual diameters. Also, the structure for diameters would then be free to include diameters for neutral solute species. Although such diameters are not be used in the B-dot model, they might be usable in other models.

5.2.5 Rescaling Ionic Activity Coefficients

The activity coefficient models described above include descriptions of individual ion activity coefficients. This is problematic in that ionic activity coefficients and ionic activities are not measurable for individual ions. These quantities are measurable only in combinations that correspond to electrical neutrality. For activity coefficients, examples of such combinations include $\log \gamma_{H^+} + \log \gamma_{Cl^-}$ and $2 \log \gamma_{H^+} + \log \gamma_{SO_4^{2-}}$; examples for activities are analogous. Molalities of individual ions are measureable (or quantifiable by inference). Thus, if one could obtain or specify the activity or activity coefficient of one single ion in an aqueous solution, one could then use this as a reference to obtain the activities and activity coefficients of all other ions present in the same solution.

The need to define activity coefficients and activities for individual ionic species is dealt with by the use of a "splitting" convention. Such a convention is at least somewhat arbitrary, although it may be guided in part by theoretical concerns. One could address the issue by adopting the results of model equations for single ion activity coefficients. The model equations for these are all in part arbitrary, implicitly including a splitting based on some combination of theoretical notions and pleasing (but not necessarily unique) symmetry. The problem with just using the model equations in their native form is that other conventions have been previously adopted into measurement practice, particularly the measurement of pH. For accurate modeling consistent with standard analytical chemistry practice, it becomes necessary to rescale the results of the model equations presented above. This only affects the activity coefficients of ionic species. For most analytical splitting conventions, some expression is specified for the activity coefficient of a reference ion, usually Cl^- or H^+.

The most significant analytical splitting conventions for aqueous ions are tied to the definition of the pH. Conceptually,

$$pH = -\log a_{H^+}. \tag{5.30}$$

In order to provide a practical basis for measuring the pH, it is necessary to define the activity of the hydrogen ion. The splitting convention used for this purpose then defines a pH scale. The choice of pH scale further affects the definition of the redox potential, E_h.

In modern work, the dominant pH scale is the NBS scale, originated by the National Bureau of Standards, now the National Institute of Standards and Technology. The NBS scale is based on the Bates-Guggenhiem equation (Bates, 1964):

$$\log \gamma_{Cl^-} = -\frac{A_{\gamma,10}\sqrt{\bar{I}}}{1 + 1.5\sqrt{\bar{I}}}. \tag{5.31}$$

This is a simple form of the extended Debye-Hückel equation. It defines the activity coefficient of the chloride ion. It may be surprising that chloride is used as the reference ion rather than the hydrogen ion, which is more closely tied to the pH. What is apparent is that the Bates-Guggenheim equation must give a result that is different from what would be obtained for the chloride ion using say the Davies equation or the B-dot equation, or for that matter, from Pitzer's equations. In the range of low ionic strength (say less than 1 molal), the differences should be numerically small for each of the three practical models, as they and the Bates-Guggenheim equation all include some form of extended Debye-Hückel model and thus are all consistent with the Debye-Hückel limiting

law. At higher ionic strength, however, the differences can be substantial (the equivalent of several pH units).

The Bates-Guggenheim equation can be applied whether or not there is any chloride in aqueous solution, as the equation is sufficient to calculate the specified activity coefficient. The charge number of -1 is effectively built into the equation.

The Bates-Guggenheim equation (the NBS pH scale) is effectively built in to the calibration of all modern means of measuring the pH, whether in pH calibration buffers or pH paper. EQ3/6 for example by default rescales ionic activity coefficients computed from the models to be consistent with the NBS pH scale (other options, including no rescaling, may be offered). Rescaling from one scale (scale "1") to another (scale "2") is accomplished using

$$\log \gamma_i^{(2)} = \log \gamma_i^{(1)} + \frac{z_i}{z_j} \left(\log \gamma_j^{(2)} - \log \gamma_j^{(1)} \right). \tag{5.32}$$

Here j denotes the reference ion (here Cl^-) and i denotes any ion (including the reference ion). In the present context, scale "1" is usually that implied by a model equation and scale "2" is the desired scale.

An alternative convention is to choose

$$\log \gamma_{H^+} = 0. \tag{5.33}$$

For the hydrogen ion, this results in

$$pH = -\log m_{H^+}. \tag{5.34}$$

as the activity and molality of the hydrogen ion are numerically equivalent. The rescaling of ionic activity coefficients for consistency does not give an analogous result for other ions. EQ3/6 allows rescaling using this convention as an option, but it has limited utility and it not recommended as a general option in the present toolset.

The definition of the pH in terms of molality ("pmH") is significant independent of rescaling. Thus one has simply

$$pmH = -\log m_{H^+}. \tag{5.35}$$

In concentrated electrolyte solutions (e.g., WIPP, Hanford tanks), pmH is often more useful for assessing the acidity/basicity of a solution than the NBS pH. The NBS pH cannot be accurately measured in concentrated solutions owing to liquid junction effects with electrodes and interferences with dyes. Also, the Bates-Guggenheim equation (and the NBS pH scale itself) was originally intended for use only at low ionic strength. Bates (1964) suggested application to solutions with ionic strengths of no greater than 0.1 molal. Since then, however, the scale has been used at higher ionic strengths. This has led to the problem that of two highly concentrated solutions with an NBS pH of say 2, one might be acidic (in the sense that H+ is abundant) and the other not (in the sense that H+ is not abundant). In other words, the common association of pH values with various degrees of acidity/basicity (e.g., 7 is neutral) no longer applies.

Still other conventions and scales exist. However, for the present toolset only the following is required. First, the default behavior will be to apply rescaling to the NBS scale. Second, the option

will be available to use the basic model results without rescaling. Third, the pmH will be directly calculated and included in the output. An option to rescale the activity coefficients for consistency with the $\log \gamma_{H^+} = 0$ convention will not be required.

5.3 Sorption

5.3.1 Overview

Sorption involves the attachment of dissolved and/or colloidal species to mineral or other solid surfaces. Sorption has the effect of slowing the effective transport rate of a species through porous media through its retardation effect. The retardation effect for a species, R_f, is given by (Bouwer, 1991)

$$R_f = \frac{V_{gw}}{V_{sp}}, \tag{5.36}$$

where V_{gw} is the velocity of the groundwater and V_{sp} is the velocity of the species. A variety of models have been used to describe sorption and can be broadly divided into those that describe it as a bulk process versus those that are mineral or solid phase specific. The latter approach involves the calculation of bulk sorption from the sum of sorption on individual solid phases, an assumption referred to as *Component Additivity*. Within the class of bulk sorption models, a distinction can be made between those which assume a finite number of sorption sites (these are referred to as showing Langmuir type behavior and include the Langmuir isotherm itself and most surface complexation and ion exchange models) and those that assume either an infinite sorption capacity or at least a capacity that is not tightly constrained (these include the linear distribution coefficient and the nonlinear Freundlich isotherm). Alternatively, one could also distinguish between single component, non-competitive models (e.g., Langmuir and Freundlich) and multicomponent competitive models (surface complexation and ion exchange).

Another possible distinction is between equilibrium and kinetic sorption models. In many cases, the formulations for the equilibrium and kinetic cases differ only insofar as the kinetic case involves involves a thermodynamic driving force (as in the equilibrium case), but modified by a finite rate constant. In some cases, however, sorption is described as irreversible, which implies that there is no back reaction (desorption).

5.3.2 Process Model Equations

Linear Distribution Coefficients (K_d). A simple approach to describe metal or ionic radionuclide sorption by a sediment,

$$A_{aq} \leftrightharpoons A_{ads}, \tag{5.37}$$

is to use a constant distribution coefficient, defined by:

$$K_d = \frac{[A_{ads}]}{[A_{aq}]}, \tag{5.38}$$

where K_d is the distribution coefficient (L/kg), $[A_{ads}]$ is the sorbed concentration (mol/kg) to the bulk solid phase, and $[A_{aq}]$ is the total dissolved concentration in groundwater (mol/L) (Davis and

Kent, 1990). One of the key advantages of representing sorption with a distribution coefficient is that it can be easily incorporated into reactive transport models used for migration predictions.

Equation (5.38) shows that if one assumes that the amount of sorption is proportional to the dissolved concentration, then there is a linear relationship where the K_d value is the slope. In this simple case, referred to as a linear isotherm, retardation of a concentration front in simple porous media is given by

$$\frac{\bar{v}}{\bar{v}_c} = 1 + \frac{\rho_b}{n} K_d, \tag{5.39}$$

where ρ_b is the bulk density, n the porosity, $\bar{v}$ the average linear velocity of the groundwater and $\bar{v}_c$ the velocity of the point on the concentration profile where the concentration is half that of the input concentration (Freeze and Cherry, 1979). Note that the ratio $\bar{v}/\bar{v}_c$ here is the retardation factor and represents the retardation of the movement of front relative to the flowing groundwater. While this is a simplified example, it serves to illustrate the key point that the K_d value directly influences predictions of adsorbing metal or radionuclide mobility.

Assumptions and Applicability Sorption is proportional to the dissolved concentration. The aqueous and adsorbed phases are in equilibrium.

Data Needs Typically K_d values are determined for a particular subsurface material from the slope of a fitted line to the concentration of the sorbed species, A_{ads}, plotted versus the dissolved concentration of the same species, A_{aq}. These data may be derived from laboratory analyses, where one typically varies the dissolved concentrations systematically, or they may be derived from in situ field data. Since K_d values may be variable, and in particular a function of temperature, pH or the redox state of the system (see below), it is often necessary to compile them in a lookup table for use by a particular computer code.

Langmuir Isotherm. The Langmuir isotherm assumes that the sorption sites, S, on the surface of a solid (absorbent) become occupied by an absorbate from the solution, A. Implying a 1:1 stoichiometry

$$S + A \leftrightharpoons SA, \tag{5.40}$$

where SA is the adsorbed species on the surface. At equilibrium, a standard mass action equation can be written:

$$K_{ads,L} = \frac{[SA]}{[S]\{A\}}, \tag{5.41}$$

where the square brackets here refer to the concentration of the species or site, and the curly brackets refer to the aqueous activity. Using the maximum concentration of surface sites, S_T

$$[S_T] = [S] + [SA], \tag{5.42}$$

one can write the Langmuir isotherm in its familiar hyperbolic form

$$[SA] = [S_T] \frac{K_{ads}\{A\}}{1 + K_{ads}\{A\}}. \tag{5.43}$$

Assumptions For the following, it is assumed that the surface and aqueous species are in equilibrium.

Data Needs The equilbrium constant, K_{ads}, is typically obtained from experimental data. It depends on the specified absorbent and absorbate, and may be a function of temperature. It may be calculated from:

$$K_{ads} = \exp\left(\frac{-\Delta G^{\circ}_{ads}}{RT}\right), \tag{5.44}$$

where ΔG is the change in free energy for the reaction, typically obtained from a database, R is the gas constant and T is the temperature.

Freundlich. The Freundlich isotherm is another equilibrium model for sorption of absorabte A onto sorption sites, S

$$S + A \leftrightharpoons SA. \tag{5.45}$$

Represented by the mass action equation:

$$K_{ads,F} = \frac{[SA]}{\{A\}^{\beta_F}}, \tag{5.46}$$

where the square brackets again refer to the concentration of the species or site, the curly brackets refer to the aqueous activity. $K_{ads,F}$ and β_F are the Freundlich parameters (e.g. Langmuir, 1997; Stumm, 1992).

Assumptions For the following, it is assumed that the surface and aqueous species are in equilibrium.

Data Needs The Freundlich parameters, $K_{ads,F}$ and n, are generally obtained by fits to experimental data for a specific surface and aqueous species. They will generally be obtained from a database, and may be represented by a functional form or lookup table.

Multi-site, Multi-component Ion Exchange. An ion exchange reaction can be described via a mass action expression with an associated equilibrium constant (Appelo and Postma, 1993; Sposito and Sparks, 1981; Vanselow, 1932). The exchange reaction can be written in generic form as

$$vACl_u(aq) + uBX_\nu(s) \leftrightharpoons uBCl_\nu(aq) + vAX_u(s), \tag{5.47}$$

where X refers to the exchange site occupied by the cations A^{u+} and B^{v+}. The equilibrium constant, K_{eq}, for this reaction can be written as (Vanselow, 1932)

$$K_{eq} = \frac{\{BCl_\nu\}^u \{AX_u\}^\nu}{\{ACl_u\}^\nu \{BX_\nu\}^u}, \tag{5.48}$$

where the curly braces refer to the thermodynamic activities. Several activity conventions are in wide use. One possibility is the Gaines-Thomas activity convention, which assumes a reaction

stoichiometry of the following form (Appelo and Postma, 1993), written here assuming the Cs^+ is the relevant cation of interest

$$Cs^+ + (1/z)MX(i)_z \leftrightharpoons CsX(i) + (1/z)M^{z+}, \tag{5.49}$$

where M is the competing cation (Na^+, K^+, Ca^{++}), z is its charge, and $X(i)$ refers to the i^{th} type of exchange site. In the Gaines-Thomas convention, each exchange site, $X(i)$ has a charge of -1. The activities of adsorbed species correspond to the charge equivalent fractions, $\beta(i)_M$,

$$\beta(i)_M = \frac{z_M q(i)_M}{\sum_M z_M q(i)_M} = \{X(i)_M\}, \tag{5.50}$$

where z_M is the charge of cation M, $q(i)_M$ is the concentration of adsorbed cation M in exchange site *i* (moles/g), and the curly brackets denote activities. The Gapon activity convention is obtained by writing the reactions in every case with a single exchanger (Appelo and Postma, 1993). Alternatively, the Vanselow convention (Vanselow, 1932) describes the exchanger activity with mole fractions

$$\beta(i)_M = \frac{q(i)_M}{\sum_M q(i)_M} = \{X(i)_M\}. \tag{5.51}$$

The exchange reactions can then be used to write a mass action equation for binary Cs-M exchange:

$$K_{M/Cs} = \frac{\beta(i)_M^{1/z}\{Cs^+\}}{\beta(i)_{Cs}\{M^{z+}\}^{1/z}} \tag{5.52}$$

$$= \frac{\{X(i)_M\}^{1/z}\{Cs^+\}}{\{X(i)_{Cs}\}\{M^{z+}\}^{1/z}}. \tag{5.53}$$

In a single-site ion exchange model, the CEC is equal to the sum of the charge equivalent concentrations of the adsorbed cations:

$$CEC = \sum_M z_M q_M, \tag{5.54}$$

while in a multi-site model, the CEC is the charge summed over all of the cation exchange sites (Cernik et al., 1996; Voegelin et al., 2000)

$$CEC = \sum_i \sum_M z_M q(i)_M. \tag{5.55}$$

Assumptions For the following, it is assumed that the surface and aqueous species are in equilibrium.

Surface Complexation. An alternative approach that allows a modeler to describe sorption while simultaneously considering variable chemical conditions in the subsurface is a surface complexation model (Davis et al., 2004). In this approach, the sorbing sediment surfaces are considered to possess surface functional groups that can form complexes analogous to the formation of aqueous complexes in solution. These surface reactions include proton exchange, cation binding and anion

binding via ligand exchange at surface hydroxil sites (represented here as XOH to avoid confusion with other chemical species). For example, the sorption of a metal could be represented as

$$XOH + M^{z+} \leftrightharpoons XOM^{z+-1} + H^{+}. \tag{5.56}$$

At equilibrium, the sorption reactions can be described by the mass law equation

$$K_{app} = \frac{[XOM^{z+-1}]\,\{H^{+}\}}{[XOH]\,\{M^{z+}\}}, \tag{5.57}$$

where K_{app} is referred to as the apparent equilibrium constant, because it includes surface charge effects and hence is dependent on the extent of surface ionization (Dzombak and Morel, 1990), $\{i\}$ is the thermodynamic activity of aqueous species i, and the terms in square brackets represent the concentration of surface complexes (mol/kg).

Surface complexation differs from the simpler isotherm and ion-exchange models in several important ways. Surface complexation is based on the electrical double layer (EDL) theory. EDL theory assumes that the surface charge of a sorbent in contact with solution generates an electrostatic potential that declines rapidly away from the sorbent surface, creating an electrostatic field. An additional energetic term accounting for the work needed for the aqueous species to travel across the surface electric field is required:

$$\begin{aligned} \Delta G_{ads} &= \Delta G_{intr} + \Delta G_{coul} \\ &= \Delta G_{intr} + (\Delta G_{\psi=0} - \Delta G_{\psi=\psi_0}) \\ &= \Delta G_{intr} - zF\psi_0. \end{aligned} \tag{5.58}$$

where ΔG_{ads} is the free energy change of the overall adsorption reaction, ΔG_{intr} and ΔG_{coul} are the free energy change due to chemical bonding and to the electrostatic work (Coulombic attraction), respectively, z is the charge of the surface species, F the Faraday's constant (96485 C/mol), and ψ_0 is the mean surface potential (V). Since

$$\Delta G = -RTlnK, \tag{5.59}$$

Equation (5.58) can be rewritten as

$$K_{app} = K_{int} \exp\left(\frac{zF\psi_0}{RT}\right), \tag{5.60}$$

where R is the gas constant (8.314 J/mol/K), T is the absolute temperature (K), and K_{int} is the intrinsic equilibrium constant which does not depend on the surface charge.

Bulk and Mineral Specific Surface Complexation. There are two major approaches for applying the surface complexation concept to soils and sediments: the Component Additivity (CA) and Generalized Composite (GC) approaches (Davis et al., 1998, 2004). In the CA approach, it is assumed that a mineral assemblage is composed of a mixture of one or more reference phases, whose surface chemical reactions are known from independent studies of each phase (e.g. Arnold et al., 2001; Davis et al., 2004; Landry et al., 2009). Based on a measurement of the relative amounts or

surface areas of each mineral present in the soil or sediment, sorption by the mixture of phases can be predicted by an equilibrium calculation, without any fitting of experimental data for the mixture. CA model predictions are sometimes made by assuming that one mineral component dominates sorption (Barnett et al., 2002; Davis et al., 2004; Payne et al., 2004; Zhang et al., 2009), allowing a straightforward equilibrium calculation, if the exposed surface area of that mineral component in the soil or sediment can be quantified.

In the GC approach, the surface of the mineral assemblage is considered too complex to be quantified in terms of the contributions of individual phases to sorption and/or that the contribution of individual components is not additive. The complexity is caused, in part, by the difficulties in quantifying the electrical field and proportions of surface functional groups at the mineral-water interface in the mixture of mineral phases and associated surface coatings. In the GC approach, it is assumed that sorption can be described by mass laws written with "generic" surface functional groups, with the stoichiometry and formation constants for each mass law determined by fitting experimental data for the mineral assemblage as a whole (Bond et al., 2008; Davis et al., 2004; Hyun et al., 2009). The GC modeling approach has generally been applied using a non-electrostatic model (NEM), which considers surface equilibria strictly as chemical reactions without explicit correction for electrostatic attraction or repulsion (Davis et al., 2004; Kent et al., 2000; Yabusaki et al., 2008). In an NEM, the apparent binding constants and stoichiometry of the mass action equations are derived by fitting the *macroscopic* dependence of adsorption as a function of pH (Davis et al., 1998). Because of the exclusion of electrical double layer terms, the mass action equations are not expected to provide accurate representations of the stoichiometry of the reactions *at the molecular scale*, however, the surface reactions can still be coupled with aqueous complexation reactions to provide simulations of macroscopic sorption as a function of aqueous chemical conditions.

Although there are differences between the GC and CA approaches, they are very similar with respect to their scientific basis. The following concepts form the basic tenets of both GC and CA modelling approaches (Davis et al., 1998):

1. Mineral surfaces are composed of chemical functional groups that can react with dissolved solutes to form surface complexes (coordinated complexes or ion pairs) in a manner analogous to aqueous complexation reactions in homogeneous solutions.

2. The equilibria of surface complexation and ionization reactions can be described via mass law equations, either with or without correction factors applied for electrostatic attraction to or repulsion from the surface.

3. The apparent binding constants determined for the mass law equations of surface complexation and ionization reactions are semi-empirical parameters related to thermodynamic constants via rational activity coefficients for surface species.

Both CA and GC models may:

1. be coupled to the same critically reviewed aqueous thermodynamic data

2. use spectroscopic data to constrain and/or determine surface complex chemical composition and stoichiometry, and

3. use the same mass laws and surface species.

The differences among the model approaches lie primarily in the manner in which the models are calibrated and assumptions about various model parameters (in particular, whether the contributions of the various mineral phases to sorption and electrostatic fields can be considered as additive). CA models have almost always been applied using mass laws with electrostatic correction factors, while GC models have not usually used these factors.

Experimental and Modeling Issues Associated with SCMs for Soils and Sediments. Common to all applications of surface complexation approaches in soils and sediments is an initial characterization with respect to surface area, bulk mineralogy, and clay and organic carbon content. In addition, if the sediment is already contaminated with a metal or radionuclide, a measurement of the labile fraction of the contaminant needs to be determined (Bond et al., 2008; Curtis et al., 2004; Kohler et al., 2004).

In the GC approach, laboratory experiments are conducted with the field site sediments across the range of chemical conditions that are relevant to the scenarios of the physical and temporal modeling domains. Then, mass law relationships are derived that describe the change in metal or radionuclide sorption with variations in the aqueous chemical conditions (Davis et al., 2004). Total surface functional groups are typically estimated from surface area measurements. The number of surface site types and surface binding reactions is a practical modeling decision made based on the goodness-of-fit and the desired number of modeling parameters (Hyun et al., 2009).

In the CA modeling approach, after the sediment mineralogy is known, an estimate of the distribution of mineral surface areas is made. This can be done by simply assuming that the bulk weight abundances of various mineral phases are related to the distribution of functional groups at the sediment surface. For example, if quartz represents 60% by weight of the sediment, then an initial estimate could be that 60% of the surface area is represented by the quartz surfaces. Then a model of metal or radionuclide adsorption on quartz (as a function of chemical conditions relevant to the field site) is chosen from available literature data. Similar models for other minerals in the sediment are also catalogued. In some cases, model parameters may need to be re-derived from the original experimental data to develop a dataset that is self-consistent. In particular, this may be necessary if different electrical double layer models were used in the reference mineral models. Other approaches for estimating the distribution of mineral surface areas may be used, including chemical extractions and other methods (Davis et al., 1998, 2004). Once the component mineral models have been chosen, a predictive calculation of metal or radionuclide sorption for a specific set of chemical conditions can be made.

Possible limitations inherent to the surface complexation approach include poor representation of: a) surface functional groups, b) surface area, c) electrical double layer properties, d) surface species, e) surface binding constants, and f) competing surface reactions and their electrostatic effects. These limitations exist for both GC and CA modeling approaches, but the GC approach attempts to resolve some of the issues by using empirical data to overcome unknown factors and unmeasured parameters. For example, consider the representation of surface functional groups: Assume that only silanol, aluminol, ferrinol, and clay mineral edge sites are of importance in a particular sediment sample. At present it is very difficult or expensive to determine the distribution of mineral surface areas in a mixed mineral assemblage. Extractions, X-ray diffraction, and

surface spectroscopies have been used by various investigators, but each of these methods provides estimates that are difficult to confirm independently. This uncertainty is circumvented in the GC approach by assuming that the distribution of site types is an unknowable quantity, and only generic sites are used. However, this requires that experimental data for the metal or radionuclide sorption on a site-specific sediment sample are collected, whereas in principle at least, additional characterization experiments are not needed for the CA modeling approach.

Quantifying Surface Sites Surface area is an important experimental quantity to be characterized in all surface complexation approaches. Typically a mixed mineral assemblage is characterized by BET analysis of nitrogen gas adsorption. Adjustments may need to be made for samples that contain high abundances of clay minerals, depending on whether there is evidence of sorption on the basal planes of clay mineral particles. Many investigators have concluded that surface functional groups of the basal planes are unreactive for metal and radionuclide sorption, and therefore the surface area of the basal planes does not need to be included in most applications. Fortunately, the BET method does not typically measure the surface area of the basal planes. In GC applications, the surface area is typically used in a straightforward manner to quantify the total abundance of surface sites using a conversion factor. In CA applications, however, the surface area should be distributed among different functional group types.

Multiple site-types are commonly used in formulating SCMs and approximate the nonlinear isotherms commonly observed for cation adsorption on well-characterized oxide mineral phases (Davis and Kent, 1990; Dzombak and Morel, 1990). Postulating multiple site-types is also important for simulating peak tailing observed in experimental studies of U(VI) transport in columns (Kohler et al., 1996). Reactive transport simulations that use multisite adsorption models can also simulate significant peak tailing in field-scale simulations (Curtis et al., 2006; Kent et al., 2000, 2008, 2007).

Sub-models

1. **Non-electrostatic Models:** EDL models differ in whether coulombic attraction or repulsion terms are considered in the mass laws of surface reactions. A non-electrostatic EDL means that the term

$$\exp\left(\frac{zF\psi_0}{RT}\right) \tag{5.61}$$

in Equation (5.60) need not be considered. While electrical double layer (EDL) models may represent these terms well for simple systems with single mineral phases, the approaches for treating these terms in mixed mineral assemblages have not been studied. In Component Additivity (CA) (Davis et al., 1998, 2004) applications to sediments, typically authors assume that the EDL properties of pure, clean mineral phases investigated remain the same in mixed mineral assemblages (Davis et al., 2004). This ignores the likely effects of surface contaminants (adsorbed major solutes such as silicate, organic compounds, etc.) and the overlapping EDL regions of particles that are known to change coulombic terms. In Generalized Composite (GC) approaches (Davis et al., 1998, 2004), the coulombic attraction or repulsion terms are not included, but are instead built into the semi-empirical model calibration of reaction stoichiometries and binding constants to experimental data. That is,

whatever EDL forces exist, they are lumped into the model fitting of reactions and binding constants. In each case, there is inherent uncertainty in the modeling approach. The errors within the GC model may not be that significant because of model calibration to experimental data, but the error is only minimized by confining model calculations to chemical conditions interpolated between those investigated in laboratory experiments. Extrapolation of any non-electrostatic model to uninvestigated chemical conditions is unwise because the EDL forces for those conditions will not necessarily be captured accurately by the model calibration. In addition the formation of unknown surface species may not be realized if calculations are extrapolated to chemical conditions not investigated at all.

2. **Electrostatic models:** When the coulombic attraction or repulsion terms is considered as shown in Equation (5.60), the electrostatic models differs also among themselves in how they conceptualize the structure of the double-layer and describe changes in surface potential and surface charge from the surface of the sorbent phase to the bulk solution. In the constant capacity and diffuse-layer models, all adsorbed species are considered specifically adsorbed at the zero plane while the triple layer model can assign adsorbed species to either a zero plane or more distant plane. The constant capacity and diffuse-layer model are elaborated in the following sections.

   (a) **Constant Capacitance** The constant capacitance model is a special case of the diffuse-layer model. Both models are based on the assumption that all the species are adsorbed in the same layer and a diffuse layer of counterions constitutes the transition to homogenous solution. Additionally, it is assumed that the surface potentials are small, or the double layer has been compressed (very high ionic strength). However, differently from the diffuse-layer model, the relationship between the surface charge and the potential is assumed to be linear:

   $$\sigma = \mathbb{C}\psi, \tag{5.62}$$

   where σ is the surface charge, $C\ m^{-2}$, ψ is the potential at the surface, V, and $\mathbb{C}$ is a constant capacitance value, $C\ V^{-1}\ m^{-2}$, to be obtained from fitting experimental data. Equation (5.62) is solved for the potential and substituted into Equation (5.60).

   (b) **Diffuse Double Layer Model** The diffuse layer model has been described in great detail by Dzombak and Morel (1990) and was applied to adsorption of metals on iron oxide surfaces. In the diffuse layer model, the solid-water interface is composed of two layers: a layer of surface-bound complexes and a diffuse layer of counter ions in solution. The surface charge is calculated from the total surface species adsorbed on the layer:

   $$\sigma_p = \frac{F}{A}\sum_{k=1}^{N_s} z_k y_k. \tag{5.63}$$

   Here A is the surface area sorbent per liter solution (m^2/L), F is the Faraday constant ($96,480 C/mol$), z_k is the charge of the ion, and y_k is the concentration (mol/L) of surface bound ions in the Stern Layer. According to the Gouy-Chapman theory, the surface charge density σ_p (C/m^2) is related to the potential at the surface (volts) by:

   $$\sigma_p = (8RT\epsilon_R\,\epsilon_0\,C_e \times 10^3)^{1/2} \sinh\left(\frac{zF\psi_0}{2RT}\right), \tag{5.64}$$

where R is the molar gas constant (8.314 $Jmol^{-1}K^{-1}$), C_e is the molar electrolyte concentration (M), z is the electrolyte charge, T is the absolute temperature (K), ϵ_R is the relative dielectric constant of water ($\epsilon = 78.5$ at $25°C$), and ϵ_0 is the permittivity of free space ($8.854 \times 10^{-12}\ C\ V^{-1}m^{-1}$). Equation (5.64) is only valid for a symmetrical electrolyte, the anion and cation must have the same charge. Note that C the unit (coulombs or celcius) is not a concentration. Capacitance is not solved for explicitly, but is implicitly accounted for in Equation (5.64). It is common to use the linearized version of Equation (5.64) for low values of the potential:

$$\sigma_p = \epsilon\ \epsilon_0 \kappa \psi_0, \tag{5.65}$$

where $1/\kappa$ (m) is the double-layer thickness defined as

$$\frac{1}{\kappa} = \left(\frac{\epsilon\ \epsilon_0 RT}{2F^2 \cdot 1000\ I} \right)^{1/2}, \tag{5.66}$$

where I is the ionic strength $mol\ L^{-1}$. The first term of Equation (5.64), $(8RT\epsilon\ \epsilon_0 C_e \times 10^3)^{1/2}$, can be rewritten at $25°C$:

$$\sigma_p = 0.1174\ C_e^{1/2} \sinh\left(\frac{zF\psi_d}{2RT} \right). \tag{5.67}$$

Therefore, in the diffuse-layer model, the value of the capacitance $\mathbb{C}$ relating the surface charge and the potential can be calculated based on theoretical considerations instead of being an experimental fitting parameter.

(c) **Triple Layer Model** The triple layer model is similar to the double layer model, but divides the sorbed species into two layers, Figure 4. Strongly sorbed species are located close to the surface, the zero plane, while weakly sorbed species reside in the beta plane, seperated from the surface by the strongly sorbed species and hydration layers (e.g. Langmuir, 1997). Further out from the surface is a diffuse layer and the bulk solution similar to the double layer.

The charge balance equation for the triple layer model is

$$\sigma_0 + \sigma_\beta + \sigma_d = 0, \tag{5.68}$$

where σ_0, σ_β and σ_d are the net surface charges in the zero, beta and diffuse planes respectively, (C/m^2). The net surface charge in the zero plane is given by:

$$\sigma_0 = \frac{F}{A} \sum_{k=1}^{N_s} z_k y_k^0, \tag{5.69}$$

where the variables are as defined in Equation (5.63) with the exception of y_k^0, which is the concentration (mol/L) bound in the zero plane. Similarly, the net surface charge of the beta plane is

$$\sigma_\beta = \frac{F}{A} \sum_{k=1}^{N_s} z_k y_k^\beta, \tag{5.70}$$

where y_k^β refers to the ions bound in the beta plane. Note that the composition of the diffuse layer is not often calculated explicitly in either Triple Layer Model or the Diffuse Double Layer Model, although a method to do so has been presented by Leroy et al. (2007).

The triple layer model assumes constant capacitances between the zero plane and beta plane, $\mathbb{C}_1$, and the beta plane and d-plane, $\mathbb{C}_2$. These are related to the surface charges and potentials by:

$$\sigma_0 = \mathbb{C}_1 (\psi_0 - \psi_\beta), \tag{5.71}$$

$$\sigma_\beta = \mathbb{C}_1 (\psi_\beta - \psi_0) + \mathbb{C}_2 (\psi_\beta - \psi_d), \tag{5.72}$$

$$\sigma_d = \mathbb{C}_2 (\psi_d - \psi_\beta). \tag{5.73}$$

5.3.3 Common Data Needs for Sorption Models

All sorption models will require access to a database of parameter values that are potentially independent of the specific contaminated site under consideration. For example, the cation exchange capacity (CEC) of a mineral like smectite or kaolinite can be described with a range of values. However, it is likely that site-specific experimental data will have to be collected and either collected in a site-specific database, or serve as the basis of a site-specific lookup table.

5.4 Mineral Precipitation and Dissolution

5.4.1 Overview

Mineral precipitation and dissolution are among the most important processes affecting the transport of contaminants in the subsurface. They represent a class of heterogeneous reactions that require a slightly different treatment than do reactions taking place within the same phase. Perhaps most importantly, a kinetic treatment of mineral reactions requires the inclusion of the interfacial area between the phases (water and mineral), or reactive surface area (see Section 5.4.5). The reactive minerals may be considered as pure, in which case their treatment is simplified by the fact that their activity is always equal to one, or they may be solid solutions, in which case their activities have to be determined as in any other solution. Minerals may be assumed to be at equilibrium with the aqueous solution, in which case they can be included in the total concentration in a fashion similar to the way in which equilibrium secondary species are (Equation (5.5)), or they may be treated kinetically. In most cases, it appears to be sufficient to treat the minerals kinetically, since the equilibrium condition can be regained by using reaction rates that are sufficiently fast relative to the time scales of interest (Steefel and MacQuarrie, 1996). This approach also offers the advantage that the minerals can potentially be removed as direct unknowns in the solution procedure within any one nonlinear iteration cycle and updated only at the end of the time step.

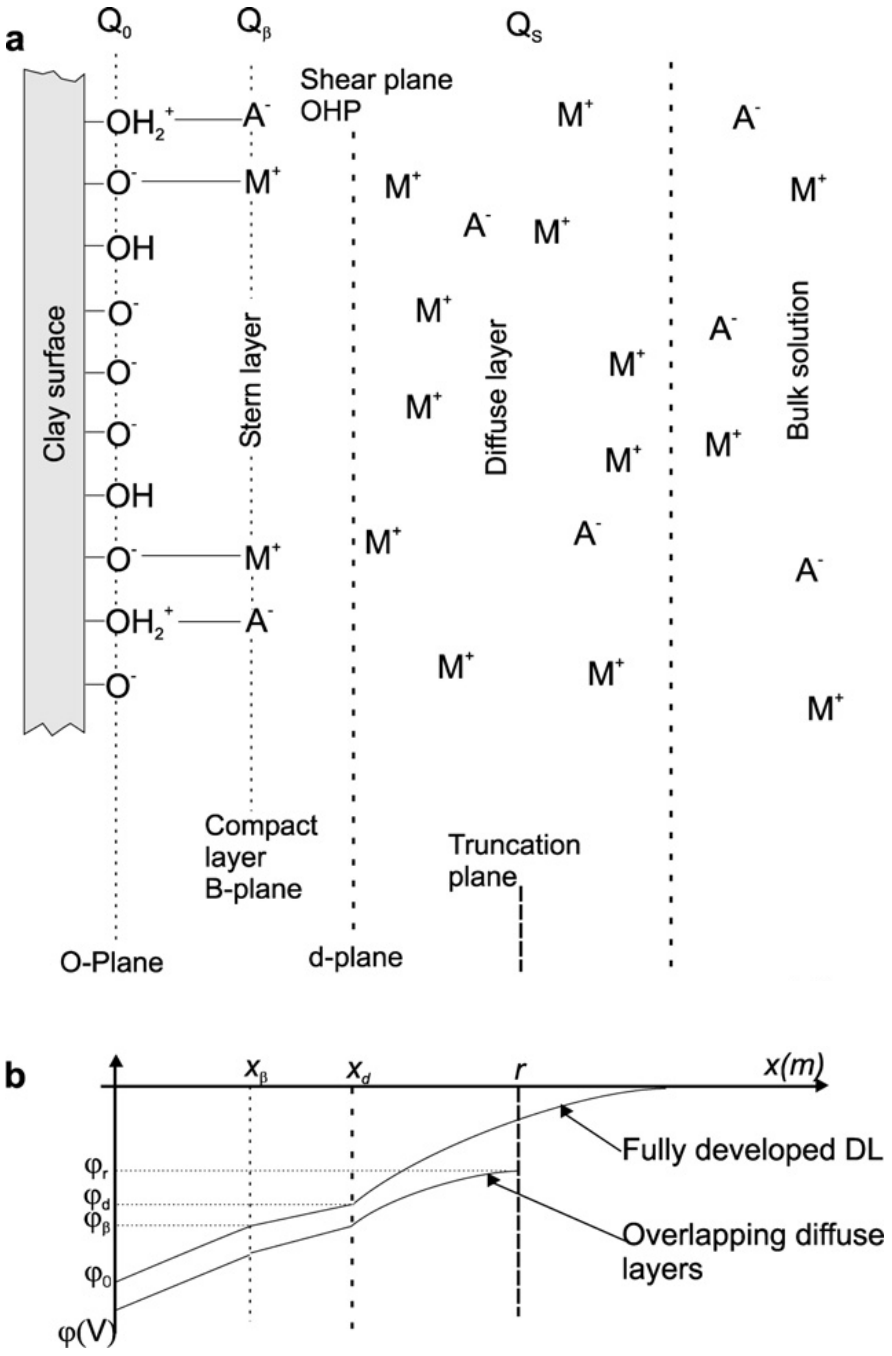

Figure 4: Schematic of the TLM model from Gonçalvès et al. (2007).

5.4.2 Kinetic Mineral-Water Rate Laws

The mineral reactions take the form

$$\sum_j \nu_{jm} \mathcal{A}_{j\alpha} \rightleftharpoons \mathcal{M}_m, \tag{5.74}$$

for mineral $\mathcal{M}_m$ with reaction rate $I_{m\alpha}$ and stoichiometric coefficients ν_{jm}. The sum of the mineral reaction rates affecting component j in phase α can be written as

$$R_{j\alpha} = \sum_m \nu_{jm} I_{m\alpha}. \tag{5.75}$$

In most cases, this will involve water as the fluid phase. Equation (5.75) implies that component j may be involved in any number of parallel mineral reaction pathways (even within the same phase), with each potentially described by its own rate law. Changes in mineral concentrations are described by the equation

$$\frac{\partial \phi_m}{\partial t} = \overline{V}_m \sum_\alpha I_{m\alpha}, \tag{5.76}$$

with molar volume $\overline{V}_m$ and where the sum over α on the right-hand side is over all fluid phases that react with the mth mineral.

We use a kinetic rate law based on the assumption that attachment and detachment of ions from mineral surfaces is the rate–limiting step (i.e., a surface reaction-controlled rate law). It does not mean, however, that one cannot obtain overall transport control on the mineral dissolution or precipitation rate since this depends on the magnitude of the reaction rate relative to the macroscopic transport rates. The rate laws used for mineral precipitation and dissolution are based loosely on transition state theory (Aagaard and Helgeson, 1982; Lasaga, 1981, 1984)).

TST Type Rate Law. This formulation gives the dependence of the rate on the saturation state of the solution with respect to a particular mineral as a function of the ion activity product, Q_s, defined by

$$Q_m = \prod_{j=1}^{N_c} a_j^{\nu_{jm}}, \tag{5.77}$$

where the a_j are the activities of the primary species used in writing the dissolution reaction for the mineral and ν_{jm} are stoichiometric reaction coefficients. In order to incorporate the strong pH dependence of most mineral dissolution and precipitation reactions far from equilibrium, parallel rate laws are used which are summed to give the overall reaction rate law for a particular mineral in phase α

$$I_{m\alpha} = -A_{m\alpha} \left\{ \sum_{l=1}^{N_{rm}} k_l \left(\prod_{i=1}^{N_c+N_x} a_i^{p_{il}} \right) \left[1 - \left(\frac{Q_m}{K_m} \right)^{M_l} \right]^{n_l} \right\}, \tag{5.78}$$

where k_l is the far from equilibrium dissolution rate constant for the lth parallel reaction, p_{il} is the exponential dependence on species i of the lth parallel reaction (i.e., the reaction order), K_m is the equilibrium constant, N_{rm} is the number of parallel reactions within phase α, and $A_{m\alpha}$ refers to

the surface area of the reacting mineral in contact with phase α (m^2 mineral m^{-3} porous medium). The exponents n_l and M_l allow for nonlinear dependencies on the affinity term and are normally taken from experimental studies. The term $\prod_{i=1}^{N_c+N_x} a_i^{p_{il}}$ incorporates the effects of various ions in solution on the far from equilibrium dissolution rate. This is most commonly the solution pH or hydroxyl ion activity but may include other electrolytes as well.

The temperature dependence of the reaction rate constant can be expressed reasonably well via an Arrhenius equation (Lasaga, 1984). Since many rate constants are reported at 25°C, it is more convenient to write the rate constant at some temperature as

$$k = k_{25} \exp\left[\frac{-\mathrm{E_a}}{\mathrm{R}}\left(\frac{1}{\mathrm{T}} - \frac{1}{298.15}\right)\right], \tag{5.79}$$

where E_a is the activation energy, k_{25} is the rate constant at 25°C, R is the gas constant, and T is temperature in the Kelvin scale.

Nonlinear Parallel Mineral Rate Laws. The rate law proposed by Hellmann and Tisserand (2006), based on experimental data for albite, can be used for dissolution of silicate minerals. One rate law describes far from equilibrium dissolution behavior with a rate constant k_2, and one rate law describes close to equilibrium behavior (k_1):

$$I_{m\alpha_\circ} = A_{m\alpha_\circ}\{k_1[1-\exp(-m_1 g^{m_2})] + k_2[1-\exp(-g)]^{m_3}\}, \tag{5.80}$$

where g represents $\frac{|\Delta G_r|}{RT}$ and the fitted parameters m_1, m_2 and m_3 have values of 7.98×10^{-5}, 3.81 and 1.17 (Hellmann and Tisserand, 2006). Here again the assumption is that the phase in question, $\alpha_\circ$, is water. This formulation is consistent with theoretical and experimental considerations which suggest that far-from-equilibrium dissolution is characterized by the opening of etch pits and rapid propagation of step waves, whereas close-to-equilibrium dissolution in the absence of etch pits is localized to surface defects.

Dissolution Only. The simplest form of a dissolution only rate law would be a completely irreversible reaction with no back reaction (i.e., no precipitation). However, it may be desirable to have a rate law which slows as equilibrium is approached, even though the back reaction cannot really be demonstrated. Such a rate law is likely applicable to the dissolution of albite at low temperature, since dissolution can be demonstrated while precipitation cannot. There is clear evidence in the case of plagioclase that the rate of dissolution does slow, so it is important to be able to include this in the code (Maher et al., 2009). Similarly, it was found that kaolinite could not be described with a single rate law that was continuous for both dissolution and precipitation (Yang and Steefel, 2008). To describe both precipitation and dissolution of kaolinite, therefore, one can use distinct dissolution-only and precipitation-only rate laws.

A rate law for dissolution only could in principle include any number of rate laws having a TST (linear or nonlinear) form, but with the added code (here presented as a linear TST rate with no dependence on dissolved or sorbed species far from equilibrium for the sake of simplicity):

$$I_{m\alpha_\circ} = \begin{cases} -A_{m\alpha_\circ}\left[1-\left(\frac{Q_m}{K_m}\right)\right] & \text{if } I_{m\alpha_\circ} < 0, \\ 0 & \text{if } I_{m\alpha_\circ} > 0. \end{cases} \tag{5.81}$$

Precipitation Only. A precipitation-only rate law takes a similar form to that of dissolution-only

$$I_{m\alpha_\circ} = \begin{cases} A_{m\alpha_\circ}\left[1 - \left(\frac{Q_m}{K_m}\right)\right] & \text{if } I_{m\alpha_\circ} > 0, \\ 0 & \text{if } I_{m\alpha_\circ} < 0. \end{cases} \tag{5.82}$$

5.4.3 Assumptions and Applicability for Rate Laws

All of the rate laws described above use reactive surface area as an important parameter (see Section 5.4.5). This is because most of the rates determined for mineral dissolution and precipitation are based on normalization to physical surface area. Rate laws that consider the actual kind and density of reactive sites are possible, but so far are difficult to implement at the field scale.

5.4.4 Data Needs for Rate Laws

Data needs for mineral dissolution and precipitation are considerable and help to explain why these processes have not always been included in subsurface environmental management codes. In the case of mineral dissolution, it is necessary to know the reactive surface area of the dissolving mineral in contact with the mobile fluid phase. Reactive surface area within immobile zones may contribute to the reactivity as well over long time scales via diffusion, so normally must be considered as well (see Section 5.4.5).

Reactive surface area is an even more difficult topic in the case of mineral precipitation. Here seeds may be created by nucleation, the seeds may growth via crystal growth and/or ripening and agglomeration (Steefel and Van Cappellen, 1990). Some proposed methods for including the evolution of reactive surface area are given in Section 5.4.5.

5.4.5 Reactive Surface Area Evolution

Surface area is a key parameter affecting mineral dissolution and precipitation rates, as well as the extent of aqueous species (e.g., contaminants) sorption onto mineral surfaces. Accordingly, surface area is one of the variables that appear in mineral dissolution and precipitation rate laws, Section 5.4, as well as in expressions needed to compute sorption site concentration for surface complexation models, Section 5.3.2. The incorporation and treatment of surface areas into reactive transport simulations can be broken down into two parts: initial surface areas, Equation (5.83), which can be either directly input into the model if known, or estimated from input geometric data and Equation (5.87) the actual evolution of surface areas (starting from input or calculated initial values) upon mineral dissolution or precipitation.

Initial surface areas can be estimated from laboratory measurements for pure minerals or bulk sediments. However, actual "reactive" surface areas in natural systems are largely unknown, and have been shown to be typically smaller than laboratory measurements by several orders of magnitude, and in much closer agreement with geometric mineral surface areas. For this reason, it is not uncommon to estimate initial reactive surface areas from available geometric data on the size and shape of mineral grains in porous media, or from data on fracture coverage (thus spacing) in fractured rocks. This can be achieved either internally or externally prior to input, using relatively

simple mathematical expressions that do not require a high level of accuracy given the large variability of this parameter in natural systems. Alternatively, initial surface areas can be calibrated during the course of reactive transport simulations.

Once initial (reactive) surface areas have been determined, the evolution of these areas upon mineral reaction needs to be captured in a manner that is consistent with field and experimental observations. For dissolving minerals in water-saturated systems, the evolution of reactive surface area can be calculated, as a first approximation, by assuming some proportionality between the amount of mineral present and its surface area. In such case, simple relationships can be developed relating surface area with mineral volume fraction, as shown further below. In unsaturated systems, however, the problem is complicated by the fact that reactive surface areas are not only function of mineral volume fractions, but also potentially of liquid saturation. While water serves as the wetting phase in most cases, and thus in in contact with the solid grains in the medium, at low saturations the coverage may become discontinuous. In this case, as a first approximation, the reactive surface area in contact with the phase (in the case of water, the "wetting phase") can be assumed to be proportional to liquid saturation.

Predicting the evolution of surface area from the onset of, and during, mineral precipitation is less straightforward. If a mineral forms on existing surfaces (of the same mineral and/or on surfaces of existing precursors), the surface area can be assumed to evolve with some proportionality to the current volume fraction of the mineral (or precursor mineral(s)). However, if a mineral actually nucleates from solution, without precursors, a rigorous treatment of nucleation is required (Steefel and Van Cappellen, 1990). Such rigorous treatment, however, is deemed outside the scope of current model requirements, primarily because input parameters for nucleation models are scarce for most minerals. Instead, an approximate treatment can be considered, yielding a trend of surface area evolution similar to that expected upon nucleation (i.e., initially large surface areas upon nucleation decreasing with growth). This general behavior can be captured by assuming that the initial (first formed, minimum) amount and grain size of a nucleating mineral is known. Using these two (input) parameters (i.e., minimum/initial volume fraction and grain size), the initial number of precipitating mineral grains and their surface area can be easily computed for each mineral assuming simple grain geometries (e.g., spheres). Upon further precipitation, the evolution of surface area can then be computed as a function of mineral grain size, with mineral grains growing with some proportionality to the amount of mineral precipitation. As such, surface areas initially decrease with increasing mineral amounts, starting from initially large values at small initial grain sizes. For each mineral, this decrease in surface area with growth can be assumed to continue until the surface area reaches some preset (input) value corresponding to the surface area of the "bulk" mineral. At this point, the surface area is assumed to evolve again with some direct proportionality to volume fraction, as in the case of dissolving minerals.

The general methodology and formulation of the above-described approach are presented further below. Note that because surface areas evolve relatively slowly in most systems, compared to other parameters such as aqueous concentrations, surface areas can be computed explicitly. That is, surface areas computed at the end of a flow/transport/reaction time step can be used as values for computing reactive transport at the next time step.

Reactive Surface Area. The following general relationship can be used to compute reactive surface areas of minerals as a function of time:

$$A_{m\alpha} \;=\; \gamma_m \;\left(\phi_m A_{SS_m}\; 1000\; \rho_m + \overline{A}_{m\alpha}\right), \tag{5.83}$$

where $A_{m\alpha}$ is the effective reactive surface area of minerals (m^2 mineral per m^{-3} porous medium), γ_m is the fraction of the mineral's surface area that is in contact with the phase (normally water), ϕ_m is the volume fraction of the mineral, A_{SS_m} is the specific surface area of the mineral (m^2/g), ρ_M is the dry density of the mineral (kg m^{-3}), and the factor of 1000 converts from kg to g. $\overline{A}_{m\alpha}$ is the precursor surface area (m^2 mineral m^{-3} medium). The fraction of the mineral surface area, γ_m, in contact with the phase α may be estimated from petrographic observations, fitted from field data, or potentially estimated based on as yet unspecified relationship with phase (liquid) saturation.

An alternative expression for computing reactive surface area is given by Steefel and Lasaga (1994)

$$A_{m\alpha} \;=\; \gamma_m A^{\circ}_{m\alpha} \left(\frac{\phi_m}{\phi^{\circ}_m}\right), \tag{5.84}$$

where $A^{\circ}_{m\alpha}$ and ϕ°_m are the initial surface area and volume fraction of the mineral, respectively.

In the case of secondary minerals that are not initially present and where no precursor mineral occurs with a non-zero volume fraction, both Eqns. (5.83) and (5.84) can be modified to include a "threshold" mineral volume fraction that is used just for the purposes of calculating reactive surface area. This mineral mass is considered to be derived from a short-lived nucleation event that quickly creates surface area upon which subsequent mineral growth can occur. The threshold volume fraction, ϕ_{nucl}, can be incorporated in the following way:

$$A_{m\alpha} \;=\; \begin{cases} \gamma_m \;\left(\phi_m A_{SS_m}\; 1000\; \rho_m\right) & \text{if } \phi_m > \phi^{nucl}_m, \\ \gamma_m \;\left(\phi_{nucl} A_{SS_m}\; 1000\; \rho_m\right) & \text{if } \phi_m < \phi^{nucl}_m. \end{cases} \tag{5.85}$$

Such a procedure obviates the need for a more complicated formulation such as that found in Steefel and Van Cappellen (1990).

Another option to be implemented involves a simple geometric method for calculating surface area (Lasaga, 1984). If a simple cubic packing of spherical grains of radius r, is considered, then the cubic arrangement of spheres yields, in a cube of side $4r$ and volume $(4r)^3$, a total of 8 spheres, each of radius r, volume $\frac{4\pi r^3}{3}$, and area $4\pi r^2$. Thus the surface area A_{nucl} (as the area of the spheres divided by the volume of the cube) can be computed as

$$A_{m\alpha} \;=\; \gamma_m \frac{0.5}{r}, \tag{5.86}$$

where r is the average grain size of the mineral. A more comprehensive approach involving crystal size distributions has been proposed by Steefel and Van Cappellen (1990).

Estimation of Reactive Surface Areas for Fractures. In a dual permeability (fracture-matrix) system, the surface area of the fracture in contact with the mobile fluid phase, A_F (in units of m^2 fracture m^{-3} medium) is (Steefel and Lasaga, 1994)

$$A_F \;=\; \varphi_F \frac{2}{\delta}, \tag{5.87}$$

where φ_F is the fracture porosity and δ is the fracture aperture. To calculate the amount of mineral surface area present along the fracture, one can use the volume fraction of the primary dissolving phase as an estimate of the fraction of the fracture surface made up of that mineral

$$A_{m\alpha} \;=\; \varphi_F \phi_m \frac{2}{\delta}. \tag{5.88}$$

For precipitation, various schemes are possible. If the assumption is made that mineral precipitation can occur anywhere along the fracture surface, then (5.87) can be used without modification. For partially wetted fractures, a correction can be introduced to reduce the reactive surface area:

$$A_{m\alpha} \;=\; \varphi_F \gamma_m \phi_m \frac{2}{\delta}, \tag{5.89}$$

where γ_m is the fraction of the fracture actually in contact with the reactive phase (normally water).

References

Aagaard, P. and H. Helgeson (1982). Thermodynamic and kinetic constraints on reaction rates among minerals and aqueous solutions; I, Theoretical considerations. *American journal of Science 282*(3), 237.

Appelo, C. and D. Postma (1993). *Geochemistry, groundwater, and pollution*. Balkema, Rotterdam.

Aris, R. (1965). Prolegomena to the rational analysis of systems of chemical reactions. *Archive for rational mechanics and analysis 19*(2), 81–99.

Arnold, T., T. Zorn, H. Zänker, G. Bernhard, and H. Nitsche (2001). Sorption behavior of U (VI) on phyllite: experiments and modeling. *Journal of contaminant hydrology 47*(2-4), 219–231.

Barnett, M., P. Jardine, and S. Brooks (2002). U (VI) adsorption to heterogeneous subsurface media: Application of a surface complexation model. *Environ. Sci. Technol 36*(5), 937–942.

Bates, R. G. (1964). *Determination of pH*. Wiley and sons, New York.

Bear, J. (1972). Dynamics of fluids in porous media.

Bond, D., J. Davis, and J. Zachara (2008). Uranium(VI) release from contaminated vadose zone sediments: Estimation of potential contributions from dissolution and desorption. In M. Barnett and D. Kent (Eds.), *Adsorption of metals by geomedia II: variables, mechanisms, and model applications*, pp. 153. Elsevier Science Ltd.

Bourg, I., G. Sposito, and A. Bourg (2008). Modeling the diffusion of na+ in compacted water-saturated na-bentonite as a function of pore water ionic strength. *Applied Geochemistry 23*(12), 3635–3641.

Bouwer, H. (1991). Simple derivation of the retardation equation and application to preferential flow and macrodispersion. *Ground Water 29*(1), 41–46.

Bowen, R. M. (1968). On the stoichiometry of chemically reacting materials. *Archive for Rational Mechanics and Analysis 29*(2), 114–124.

Brooks, R. and A. Corey (1964). Hydraulic properties of porous media.

Burdine, N. (1953). Relative permeability calculations from pore-size distribution data. *Trans. AIME 198*(1), 71–78.

Cernik, M., M. Borkovec, and J. Westall (1996). Affinity distribution description of competitive ion binding to heterogeneous materials. *Langmuir 12*(25), 6127–6137.

Curtis, G., J. Davis, and D. Naftz (2006). Simulation of reactive transport of uranium (VI) in groundwater with variable chemical conditions. *Water Resour. Res 42*(4).

Curtis, G., P. Fox, M. Kohler, and J. Davis (2004). Comparison of in situ uranium k_d values with a laboratory determined surface complexation model. *Applied Geochemistry 19*(10), 1643–1653.

Davies, C. W. (1962). *Ion Association*. Butterworths, London.

Davis, J., J. Coston, D. Kent, and C. Fuller (1998). Application of the surface complexation concept to complex mineral assemblages. *Environ. Sci. Technol 32*(19), 2820–2828.

Davis, J. and D. Kent (1990). Surface complexation modeling in aqueous geochemistry. In M. F. Hochella and A. F. White (Eds.), *Mineral-Water Interface Geochemistry*, Volume 23, pp. 177–260. Mineral Soc America.

Davis, J., D. Meece, M. Kohler, and G. Curtis (2004). Approaches to surface complexation modeling of uranium (VI) adsorption on aquifer sediments. *Geochimica et Cosmochimica Acta 68*(18), 3621–3641.

Dourado Neto, D., Q. de Jong van Lier, M. van Genuchten, K. Reichardt, K. Metselaar, and D. Nielsen (2011). Basic concepts in the theory of homogeneous liquids in fissured rocks. *Vadose Zone Journal 10*, 618–623.

Dzombak, D. and F. Morel (1990). *Surface complexation modeling: Hydrous ferric oxide*. Wiley-Interscience.

Freeze, R. and J. Cherry (1979). *Groundwater*. Prentice Hall, Englewood Cliffs, New Jersey.

Gonçalvès, J., P. Rousseau-Gueutin, and A. Revil (2007, December). Introducing interacting diffuse layers in tlm calculations: A reappraisal of the influence of the pore size on the swelling pressure and the osmotic efficiency of compacted bentonites. *Journal of Colloid and Interface Science 316*(1), 92–99.

Hamm, L. L. and S. E. Aleman (2000). FACT (version 2.0). subsurface flow and contaminant transport. documentation and user's guide. Technical Report WSRC-TR-99-00282, Westinghouse Savannah River Company. Savannah River Site. Aiken, SC.

Hellmann, R. and D. Tisserand (2006). Dissolution kinetics as a function of the Gibbs free energy of reaction: An experimental study based on albite feldspar. *Geochimica et Cosmochimica Acta 70*(2), 364–383.

Hooyman, G. J. (1961). On thermodynamic coupling of chemical reactions. *Proceedings of the National Academy of Sciences of the United States of America 47*(8), 1169.

Hyun, S., P. Fox, J. Davis, K. Campbell, K. Hayes, and P. Long (2009). Surface complexation modeling of U (VI) adsorption by aquifer sediments from a former mill tailings site at Rifle, Colorado. *Environmental Science & Technology*, 5465–5478.

Kang, Q., P. Lichtner, and D. Zhang (2006). Lattice Boltzmann pore-scale model for multicomponent reactive transport in porous media. *J. Geophys. Res 111*, B05203:1–12.

Kent, D., R. Abrams, J. Davis, J. Coston, and D. LeBlanc (2000). Modeling the influence of variable ph on the transport of zinc in a contaminated aquifer using semiempirical surface complexation models. *Water resources research 36*(12), 3411–3425.

Kent, D., J. Davis, J. Joye, and G. Curtis (2008). Influence of variable chemical conditions on EDTA-enhanced transport of metal ions in mildly acidic groundwater. *Environmental Pollution 153*(1), 44–52.

Kent, D., J. Wilkie, and J. Davis (2007). Modeling the movement of a pH perturbation and its impact on adsorbed zinc and phosphate in a wastewater-contaminated aquifer. *Water Resources Research 43*(7), W07440.

Kirkner, D. J. and H. Reeves (1988). Multicomponent mass transport with homogeneous and heterogeneous chemical reactions: The effect of the chemistry on the choice of numerical algorithm, part 1. theory. *Water Resources Research 24*, 1719–1729.

Kohler, M., G. Curtis, D. Kent, and J. Davis (1996). Experimental investigation and modeling of uranium (VI) transport under variable chemical conditions. *Water Resources Research 32*(12), 3539–3551.

Kohler, M., G. Curtis, D. Meece, and J. Davis (2004). Methods for estimating adsorbed uranium (VI) and distribution coefficients of contaminated sediments. *Environ. Sci. Technol 38*(1), 240–247.

Landry, C., C. Koretsky, T. Lund, M. Schaller, and S. Das (2009). Surface complexation modeling of Co (II) adsorption on mixtures of hydrous ferric oxide, quartz and kaolinite. *Geochimica et Cosmochimica Acta 73*(13), 3723–3737.

Langmuir, D. (1997). *Aqueous Environmental Geochemistry*. Prentice Hall, New Jersey.

Lasaga, A. (1998). *Kinetic theory in the earth sciences*. Princeton Univ Pr.

Lasaga, A. C. (1981). Rate laws of chemical reactions. In A. C. Lasaga and R. J. Kirkpatrick (Eds.), *Kinetics of Geochemical Processes, Reviews in Mineralogy and Geochemistry*, pp. 135–169. Mineral Soc America.

Lasaga, A. C. (1984). Chemical kinetics of water-rock interactions. *J. Geophys. Res 89*(B6), 4009–4025.

Leroy, P., A. Revil, S. Altmann, and C. Tournassat (2007). Modeling the composition of the pore water in a clay-rock geological formation (Callovo-Oxfordian, France). *Geochimica et Cosmochimica Acta 71*(5), 1087–1097.

Li, L., C. Steefel, and L. Yang (2008). Scale dependence of mineral dissolution rates within single pores and fractures. *Geochimica et Cosmochimica Acta 72*(2), 360–377.

Lichtner, P. and Q. Kang (2007). Upscaling pore-scale reactive transport equations using a multiscale continuum formulation. *Water Resources Research 43*, 1–19.

Lichtner, P., S. Kelkar, and B. Robinson (2002). New form of dispersion tensor for axisymmetric porous media with implementation in particle tracking. *Water Resources Research 38*(8), 21–1 – 21–16.

Lichtner, P. C. (1985). Continuum model for simultaneous chemical reactions and mass transport in hydrothermal systems. *Geochimica et Cosmochimica Acta 49*(3), 779–800.

Maher, K., C. Steefel, A. White, and D. Stonestrom (2009). The role of reaction affinity and secondary minerals in regulating chemical weathering rates at the Santa Cruz Soil Chronosequence, California. *Geochimica et Cosmochimica Acta 73*(10), 2804–2831.

Millington, R. and J. Quirk (1961). Permeability of porous solids. *Transactions of the Farada Society 57*, 1200–1207.

Moldrup, P., T. Olesen, P. Schjonning, T. Yamaguchi, and D. Rolston (2000). Predicting the gas diffusion coefficient in undisturbed soil from soil water characteristics. *Soil Science Society of America Journal 64*(1), 94.

Mualem, Y. (1976). A new model for predicting the hydraulic conductivity of unsaturated porous media. *Water Resour. Res 12*(3), 513–522.

Navarre-Sitchler, A., C. Steefel, L. Yang, L. Tomutsa, and S. Brantley (2009). Evolution of porosity and diffusivity associated with chemical weathering of a basalt clast. *Journal of Geophysical Research-Earth Surface 114*(F2), F02016.

Neuman, S. (1990). Universal scaling of hydraulic conductivities and dispersivities in geologic media. *Water Resources Research 26*(8), 1749–1758.

Onsager, L. (1931). Reciprocal relations in irreversible processes. i. *Physical Review 37*(4), 405–426.

Payne, T., J. Davis, M. Ochs, M. Olin, and C. Tweed (2004). Uranium adsorption on weathered schist–intercomparison of modelling approaches. *Radiochimica Acta/International journal for chemical aspects of nuclear science and technology 92*(9-11/2004), 651–661.

Prigogine, I. (1968). *Introduction to Thermodynamics of Irreversible Processes*. John Wiley & Sons, Inc.

Reed, M. H. (1982). Calculation of multicomponent chemical equilibria and reaction processes in systems involving minerals, gases and an aqueous phase. *Geochimica et Cosmochimica Acta 46*(4), 513–528.

S. E. Drummond, J. (1981). *Boiling and mixing of hydrothermal fluids: Chemical effects on mineral precipitation*. Ph. D. thesis, The Pennsylvania State University, University Park, Pennsylvania.

Simunek, J. and M. van Genuchten (2008). Modeling nonequilibrium flow and transport processes using HYDRUS. *Vadose Zone J. 7*(2), 782–797.

Somerton, W., A. El-Shaarani, and S. Mobarak (1974). High temperature behavior of rocks associated with geothermal type reservoirs. In *SPE California Regional Meeting*.

Sposito, G. and D. Sparks (1981). *The thermodynamics of soil solution*. Oxford.

Steefel, C. and A. Lasaga (1994). A coupled model for transport of multiple chemical species and kinetic precipitation/dissolution reactions with applications to reactive flow in single phase hydrothermal systems. *American Journal of Science 294*(5), 529–592.

Steefel, C. and K. Maher (2009). Fluid-rock interaction: A reactive transport approach. *Reviews in Mineralogy and Geochemistry 70*(1), 485.

Steefel, C. and P. Van Cappellen (1990). A new kinetic approach to modeling water-rock interaction: The role of nucleation, precursors, and Ostwald ripening. *Geochimica et Cosmochimica Acta 54*(10), 2657–2677.

Steefel, C. I. and K. T. B. MacQuarrie (1996). Approaches to modeling of reactive transport in porous media. In *Reactive Transport in Porous Media, Reviews in Mineralogy and Geochemistry* **34**, pp. 83–125. Mineral Soc America.

Stumm, W. (1992). *Chemistry of the solid-water interface: processes at the mineral-water and particle-water interface in natural systems*. New York: John Wiley & Sons.

Sumner, M. (2000). Handbook of soil science.

van Genuchten, M. (1980). A closed-form equation for predicting the hydraulic conductivity of unsaturated soils. *Soil Sci. Soc. Am. J 44*(5), 892–898.

van Genuchten, M. and D. Nielsen (1985). On describing and predicting the hydraulic properties of unsaturated soils. *Ann. Geophys. 3*, 615–628.

van Genuchten, M. T., F. J. Leij, and S. R. Yates (1991, December). The RETC Code for quantifying the hydraulic functions of unsaturated soils. Technical Report EPA/600/2-91/065, Robert S. Kerr Environmental Research Laboratory, U.S. Environmental Protection Agency, ADA, OK.

Van Zeggeren, F. and S. Storey (1970). *The computation of chemical equilibria*. Cambridge Univ Pr.

Vanselow, A. (1932). Equilibria of the base-exchange reactions of bentonites, permutites, soil colloids, and zeolites. *Soil Science 33*(2), 95.

Voegelin, A., V. Vulava, F. Kuhnen, and R. Kretzschmar (2000). Multicomponent transport of major cations predicted from binary adsorption experiments. *Journal of contaminant hydrology 46*(3-4), 319–338.

Wolery, T. J. (1969). Thermodynamics of hydrothermal systems at elevated temperatures and pressures. *American Journal of Science 267*, 792–804.

Wolery, T. J. (1992a). *EQ3NR, A Computer Program for geochemical aqueous speciation-solubility calculations: Theoretical manual, Users Guide, and Related documentation (Version 7.0)*.

Wolery, T. J. (1992b). On the thermodynamic framework of solutions (with special refernce to aqueous electrolyte solutions. *American Journal of Science 290*, 296–320.

Yabusaki, S., Y. Fang, and S. Waichler (2008). Building conceptual models of field-scale uranium reactive transport in a dynamic vadose zone-aquifer-river system. *Water Resources Research 44*(W12403).

Yang, L. and C. Steefel (2008). Kaolinite dissolution and precipitation kinetics at 22C and pH 4. *Geochimica et Cosmochimica Acta 72*(1), 99–116.

Zhang, F., J. Parker, S. Brooks, Y. Kim, G. Tang, P. Jardine, and D. Watson (2009). Comparison of approaches to calibrate a surface complexation model for U (VI) sorption to weathered saprolite. *Transport in Porous Media 78*(2), 185–197.